Advancements in Remote Sensing Imagery Applications for Precision Management in Olive Growing: A Systematic Review

Pedro Marques [1,2,*], Luís Pádua [2,3,4], Joaquim J. Sousa [4,5] and Anabela Fernandes-Silva [1,2,3]

1 Agronomy Department, School of Agrarian and Veterinary Sciences, University of Trás-os-Montes e Alto Douro, 5000-801 Vila Real, Portugal; anaaf@utad.pt
2 Centre for the Research and Technology of Agro-Environmental and Biological Sciences, University of Trás-os-Montes e Alto Douro, 5000-801 Vila Real, Portugal; luispadua@utad.pt
3 Institute for Innovation, Capacity Building and Sustainability of Agri-Food Production, University of Trás-os-Montes e Alto Douro, 5000-801 Vila Real, Portugal
4 Engineering Department, School of Science and Technology, University of Trás-os-Montes e Alto Douro, 5000-801 Vila Real, Portugal; jjsousa@utad.pt
5 Centre for Robotics in Industry and Intelligent Systems (CRIIS), INESC Technology and Science (INESC-TEC), 4200-465 Porto, Portugal
* Correspondence: pedromarques@utad.pt

Abstract: This systematic review explores the role of remote sensing technology in addressing the requirements of sustainable olive growing, set against the backdrop of growing global food demands and contemporary environmental constraints in agriculture. The critical analysis presented in this document assesses different remote sensing platforms (satellites, manned aircraft vehicles, unmanned aerial vehicles and terrestrial equipment) and sensors (RGB, multispectral, thermal, hyperspectral and LiDAR), emphasizing their strategic selection based on specific study aims and geographical scales. Focusing on olive growing, particularly prominent in the Mediterranean region, this article analyzes the diverse applications of remote sensing, including the management of inventory and irrigation; detection/monitoring of diseases and phenology; and estimation of crucial parameters regarding biophysical parameters, water stress indicators, crop evapotranspiration and yield. Through a global perspective and insights from studies conducted in diverse olive-growing regions, this review underscores the potential benefits of remote sensing in shaping and improving sustainable agricultural practices, mitigating environmental impacts and ensuring the economic viability of olive trees.

Keywords: satellite imagery; unmanned aerial vehicles; manned aircraft vehicles; RGB; multispectral; hyperspectral; LiDAR; vegetation indices; dendrometric parameters; olive tree; precision agriculture

1. Introduction

The world's population is projected to approach 10 billion by 2050, resulting in a 50% increase in agricultural demand with moderate economic growth, exceeding the levels of the previous decade [1]. To address this growing demand, there is a need to increase agricultural production through intensified practices such as fertilization, irrigation, tillage and pesticide application [2]. However, these practices, along with the impacts of climate change, have led to a reduction in arable land, particularly affecting developing countries [3]. Predictions suggest a progressive decline per capita of approximately 50% in arable land, from 0.3 hectares in 1990 to 0.15 hectares by 2050 [3]. Climate change has also increased water demand for crop irrigation, with agriculture currently consuming around 70% of global freshwater resources [4]. Therefore, adopting sustainable agricultural approaches, including precision agriculture (PA), has become imperative [5]. PA, as a scientific effort to improve crop yields and management decisions through advanced sensors and analysis tools, integrates advanced technologies to automate various agricultural operations [6]. Originating in the late 1980s, PA has progressed with technological

advancements, incorporating features such as artificial intelligence, the Internet of Things (IoT) and novel platforms and sensors [6,7] used in the remote sensing (RS) field.

In the context of technological progress, RS data emerge as an indispensable tool extensively used in PA for sustainable agriculture management and monitoring [8]. Providing non-destructive methodologies with high spatial, radiometric and temporal resolutions, RS allows the characterization and monitoring of spatiotemporal variability for multidimensional purposes [9–13]. Over the past few decades, RS technology has played a crucial role in the development of new agricultural applications, focusing primarily on monitoring vegetation cover [14–16], assessing crop vigor conditions [17–19], estimating nutrient and water status [20–22], determining crop evapotranspiration (ET$_c$) [23–25], identifying and managing invasive plants [26–28], detecting and monitoring pest/diseases [29–31] and forecasting crop yields [32–34]. The effectiveness of RS applications in agriculture depends on several fundamental factors, including the choice of sensing platform, which can be a satellite, aircraft, unmanned aerial vehicle (UAV) or terrestrial platform; the segment of the electromagnetic spectrum used; the number and range of spectral bands; spatial, temporal and radiometric resolutions; and the energy source (passive or active sensors) [9]. Over the last few years, diverse combinations of platforms and sensors have been extensively explored across various crops, designed to fulfill the specific requirements of different agricultural applications [9].

In the context of olive trees, RS has gained extensive interest due to its multidimensional applications. With 98% of global olive production concentrated in the Mediterranean Basin, the sector's significance extends beyond consumption to historical uses of olive fruit, oil and leaves [35–37]. However, the intensive cultivation of olive trees, along with climate change, needs procedures to ensure productivity and sustainability, including spatial distribution for inventory management purposes and optimized irrigation and fertilization practices [37]. Furthermore, monitoring the incidence of diseases and other phytosanitary issues is equally crucial. Olive Anthracnose (*Colletotrichum* spp.), Canker (*Verticillium Wilt—VW*), Olive leprosy (*Phlyctema vagabunda*), Peacock Spot (*Cycloconium oleaginum*) and Oleander scale (*Aspidiotus nerii*) are among the most prominent diseases [38]. Moreover, the recent emergence of *Xylella fastidiosa* (*Xf*) poses a prominent threat, leading to significant negative impacts on olive production [39]. This has attracted the interest of the scientific community focused on the sector, motivating concerted efforts to control its expansion. RS techniques have been effectively applied in addressing this challenge [29–31]. For instance, researchers have effectively developed semi-automatic approaches, using geostatistical analysis on multispectral (MSP) data [29] with machine learning (ML) methods [40] and incorporating vegetation indices (VIs) [39] from hyperspectral (HSP) imagery. These methodologies enabled the effective monitoring and detection of *Xf* during its early developmental stages, before it becomes perceptible to the human eye. Beyond disease research, RS technology shows considerable potential for diverse applications in olive orchard management, offering valuable insights and contributing to improved agricultural practices.

Facing the imperative challenges in contemporary agriculture, there is a growing awareness of the need for a thorough examination of RS applications in the olive cultivation context. The relationship between the increasing global population, rising food demands and ongoing environmental constraints requires a re-evaluation of traditional agricultural approaches. The complex dynamics of climate change, the intensification of agricultural practices and the association between water scarcity and crop irrigation underscore the demand for innovative solutions. By offering non-destructive methodologies with high spatial, radiometric and temporal resolutions, RS has proven effective in addressing the numerous challenges faced by olive growers. Consequently, this review article aims to explore the applications of RS in olive cultivation, providing a comprehensive analysis that extends beyond the surface and emphasizing the transformative role that RS technology can play in developing sustainable and resilient agricultural practices for the future. This review allowed for the identification of three publications with similar topics [10–12]. However, the

temporal scope covered ends in 2021 [10] and March 2022 [11,12]. It was precisely in these latter two years, not covered by those works, that a significant increase in RS applications in olive orchards was observed. In fact, approximately 30% of the 218 studies considered in this review belong to 2022 and 2023. This gap is evident in the mentioned reviews, as only 56, 72, and 41 studies were considered, respectively, in [10–12]. Therefore, there is a significant need to investigate these recent contributions to evaluate the advancements of RS in this field. Additionally, the expanding range of RS applications in these years has led to the incorporation of new categories within this review. This document assesses the types of data acquired from RS imagery and explores common image processing techniques, contributing to an improved understanding of RS technologies for olive growth practices.

2. Materials and Methods

2.1. Literature Review Process
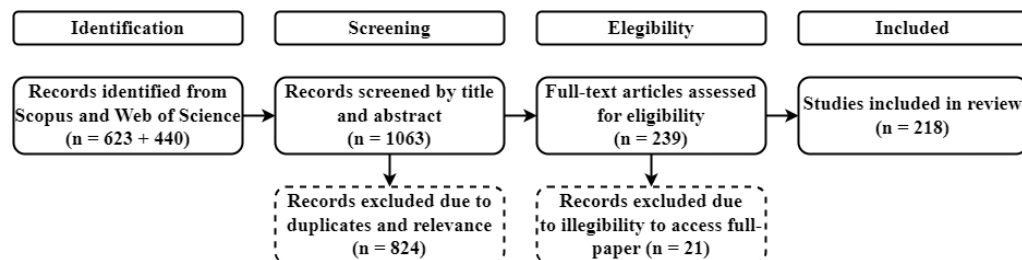
This systematic review aimed to collect peer-reviewed research studies applying RS imagery for diverse applications in olive cultivation, obtained from satellites, UAVs, aircraft and terrestrial platforms. Using a rigorous approach, both Scopus (Elsevier B.V., Amsterdam, the Netherlands) and Web of Science (Clarivate Analytics, London, UK) databases were queried without imposing temporal limitations, ensuring the inclusion of all relevant studies. Table 1 presents an overview of the queries used for each database. The queries to both databases were performed on 17 November 2023.

Table 1. Databases and queries used to define the scope of this study.

Database	Website	Query
Scopus	https://www.scopus.com/home.uri (accessed on 17 November 2023)	TITLE-ABS-KEY (olive OR olea) AND TITLE-ABS-KEY ("remote sensing" OR UAV OR satellite OR Sentinel OR MODIS OR "unmanned aerial vehicle" OR aircraft OR LANDSAT) AND (LIMIT-TO (DOCTYPE,"ar") OR LIMIT-TO (DOCTYPE,"cp") OR LIMIT-TO (DOCTYPE,"ch"))
Web of Science	https://www.webofscience.com (accessed on 17 November 2023)	TI = (olive OR olea) AND TI = ("remote sensing" OR uav OR satellite OR sentinel OR modis OR "unmanned aerial vehicle" OR aircraft OR landsat) OR AB = (olive OR olea) AND AB = ("remote sensing" OR uav OR satellite OR sentinel OR modis OR "unmanned aerial vehicle" OR aircraft OR landsat) OR AK = (olive OR olea) AND AK = ("remote sensing" OR uav OR satellite OR sentinel OR modis OR "unmanned aerial vehicle" OR aircraft OR landsat) OR KP = (olive OR olea) AND KP = ("remote sensing" OR uav OR satellite OR sentinel OR modis OR "unmanned aerial vehicle" OR aircraft OR landsat)

2.2. Result Filtering

The initial queries produced 1063 research studies. Using the Preferred Reporting Items for Systematic Reviews and Meta-Analyses (PRISMA) framework [41], as illustrated in Figure 1, the results were screened by removing duplicate publications and studies not aligning with the review's proposed goals, based on title and abstract analysis. This process excluded 824 studies, resulting in 239 publications for further analysis. A secondary manual selection process followed, excluding studies with inaccessible full papers and those outside the review's scope, resulting in the inclusion of 218 research studies, including 165 journal articles, 49 conference papers and 4 book chapters.


Figure 1. PRISMA workflow diagram of the systematic literature review process.

2.3. Study Classification and Analysis

The classification methodology aimed to offer a detailed overview of the technological scenario, as summarized in Table 2. Studies were categorized based on sensor types (RGB, MSP, HSP, thermal infrared (TIR) and light detection and ranging (LiDAR)) and platforms (satellites, UAVs, aircraft and terrestrial).
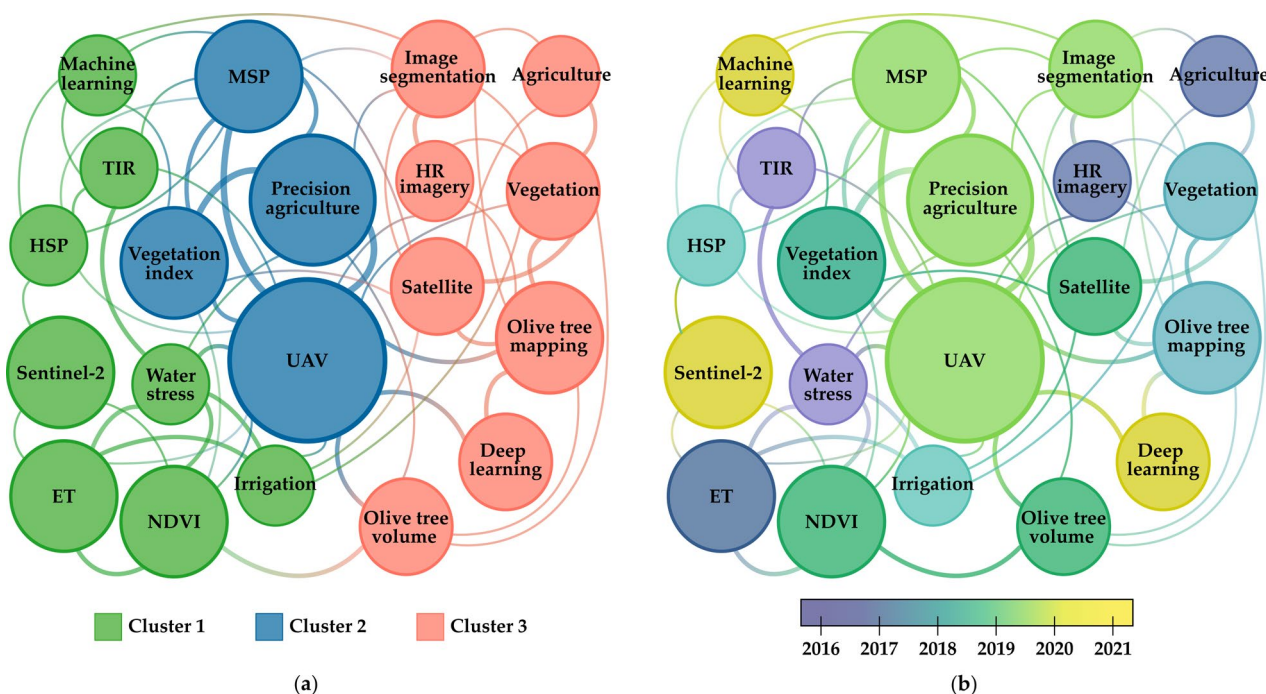
Table 2. Classification types of the research studies based on sensor types, platforms, agronomic application areas and number of studies. MSP: multispectral; HSP: hyperspectral; TIR: thermal infrared.

Class	Subclass Type
Platform	Satellite (103), UAV (88), aircraft (33) and terrestrial (6)
Sensor	RGB (182), MSP (145), TIR (58), HSP (18) and LiDAR (7)
Application category	Inventory (72), irrigation management and water stress indicator estimation (34), biophysical parameter estimation (49), crop evapotranspiration and crop coefficient estimation (26), disease detection/monitoring (22), yield estimation (10) and others (19).

Seven agronomic application areas, such as inventory management, irrigation optimization and disease detection, emphasized the multifaceted effectiveness of RS imagery in olive growing. A critical analysis of methodologies, techniques and main results was conducted, with a focus on studies published in scientific journals.

Keyword occurrence and clustering analysis was performed using the software VOSviewer (version 1.6.20), exposing relevant patterns and trends in the analysis of keywords extracted from the 218 selected research studies. Figure 2 presents a visual representation of the 20 most common keywords, excluding terms such as "remote sensing", "olive tree" and "*Olea europaea*" due to their intrinsic association with the main theme of this review. The identified clusters, categorized by color (Figure 2a), reveal the key thematic areas within the reviewed literature. In the green category, which includes terms such as "evapotranspiration", "irrigation", "water stress", "ndvi" and "thermal", an emphasis on water-related issues emerges. This cluster underlines the significance of RS in addressing challenges associated with water stress and optimizing irrigation practices in olive cultivation. The focus on thermal imagery suggests a specific interest in monitoring and managing water-related stress. Within the blue category, consisting of keywords such as "UAV", "vegetation index" and "multispectral", there is a clear indication of a growing role of UAVs in PA. Studies in this cluster used MSP data and VIs derived from UAVs, emphasizing the increasing application of these technologies for optimized agricultural practices in olive cultivation. The red category, represented by terms such as "olive tree mapping", "satellite", "image segmentation" and "olive tree volume", underscores a predominant application of RS in inventory and biophysical assessments within olive cultivation. This cluster suggests an exploration of spatial mapping, volumetric analysis and satellite-based monitoring for olive tree management.

Regarding the temporal analysis (2004–2023), distinct shifts in research focus are evident (Figure 2b). In 2016, a significant emphasis on keywords associated with water scarcity, "evapotranspiration", "water stress" and "thermal" reflects a heightened awareness of water management challenges in olive cultivation. Subsequently, from 2019 onwards, there is a prominent increase in research activities exploring UAV technologies, with a specific emphasis on topics such as "olive tree volume" and "image segmentation" using MSP images and the Normalized Difference Vegetation Index (NDVI) [42]. A recent emergence of advanced technologies such as "machine learning" and "deep learning" in the cluster analysis is evident. This suggests a contemporary trend towards applying advanced analytical approaches to improve the precision and effectiveness of RS applications in olive cultivation.

Figure 2. Keyword occurrence and clustering analysis using VOSviewer (1.6.20): (**a**) network visualization; (**b**) temporal overlay visualization. Colors indicate the year in which keywords were most frequently used. Lines represent the strength of co-occurrence links among terms. ET: evapotranspiration; HSP: hyperspectral; MSP: multispectral; NDVI: Normalized Difference Vegetation Index; TIR: thermal infrared; UAV: unmanned aerial vehicle.

3. Overview of Remote Sensing Platforms, Sensors and Image Processing Techniques

3.1. Platforms

RS includes non-contact techniques enabling the observation of areas, phenomena or objects [43]. Its primary objective is to provide observations of specific physical parameters within a mapping framework at a given time. In the agricultural context, RS is based on the interaction of electromagnetic radiation with plants and crops. Several platforms and sensors, dependent on operating wavelength and relating to biological and physical parameters in agriculture, can be used for data collection. Traditional RS technologies include satellites, aircraft, UAVs and terrestrial equipment [44], each revealing distinct advantages and limitations concerning technological, operational and economic factors.

3.1.1. Satellites

Satellite imagery was first used for agricultural purposes during the early 1970s, with Bauer and Cipra [45] pioneering its use to identify agricultural crops through computer processing. Especially in the last two decades, characterized by the launch of new space missions with improved spatial, spectra, and temporal resolutions, spaceborne RS has experienced extensive applications in agricultural contexts [45]. These platforms, benefiting from high-altitude orbits, provide extensive coverage with reasonable spectral capability [43]. In particular, these platforms contributed to detecting olive trees within study sites covering vast areas of 5600 ha [46] and 15,000 ha [47], which would be impractical with other RS platforms due to associated costs. Technological advancements and increased sensor capacity in recent missions offer multiple optical bands with higher spatial resolution and shorter revisit times. However, a trade-off exists between cost and spatial resolution. Despite the abundance of missions with numerous optical bands, non-commercial data typically demonstrate coarser spatial resolutions (≥10 m spatial resolution), making them unsuitable for several PA applications [48]. In specific cases, especially when study areas are small, the 10 m spatial resolution may prove insufficient for obtaining the desired data.

Additionally, the cost of acquiring higher-resolution imagery from commercial missions may compromise cost-effectiveness [49]. Moreover, satellites are sensitive to cloud cover, and mission orbital design determines image acquisition timing over specific regions [43]. Despite these challenges, satellite imagery is widely used in olive growing, including in inventory management, ET and crop coefficient (K_c) estimation, biophysical parameter estimation, yield estimation and phenology monitoring. However, high costs, particularly for greater spectral variety and/or high spatial resolutions, limit its use mainly to inventory and coverage area purposes. Table 3 outlines the most frequently used satellites in olive growing, along with their key technical specifications. The satellites listed in this table exclusively correspond to those used in the studies retrieved through the PRISMA workflow.

Table 3. Satellite platforms used in olive-growing applications from the identified studies.

Mission	Launch Year	Availability	Price per km² (EUR)	No. of Bands	Spectral Range (nm)	Spatial Resolution (m)	Swath Width at Nadir (km)	Study References
Landsat-5 *	1984	Free	-	7	450–12,500	30–120	185	[50–56]
IRS-1D *	1997	Collaborative	-	4	520–1750	23–70	70	[57–59]
Landsat-7	1999	Free	-	8	450–12,500	15–60	185	[50–57,60–67]
IKONOS *	1999	Commercial	9	5	445–929	0.8–4	11.3	[60,68–71]
Terra/Aqua	1999	Free	-	36	405–14,385	250–1000	2300	[27,54,60,72–78]
Quickbird *	2001	Commercial	14	5	450–900	0.6–2.6	16.8	[34,79–85]
Formosat-2 *	2004	Collaborative	1.5	5	450–900	2–8	24	[53]
RapidEye *	2008	Commercial	1.1	5	440–850	5–6.5	77	[86]
WorldView-2	2009	Commercial	15.7	9	450–800	0.5–1.8	16.4	[25,87–90]
Pleiades-1	2011	Commercial	11.2	5	430–950	0.5–2	20	[46,87,91]
Landsat-8	2013	Free	-	9	430–1390	15–100	185	[23,52,54,64,69,72,73,92–94]
SPOT-7	2014	Commercial	4.2	5	450–890	1.5–6	60	[95]
WorldView-3	2014	Commercial	20.2	29	400–2365	0.3–30	13.1	[88,89,96,97]
Sentinel-2	2015	Free	-	13	443–2190	10–60	290	[15,16,18,24,47,91,93,98–122]
PlanetScope	2016	Commercial	2	8	431–885	3–4.1	25	[86,88,102,120,121,123]
PRISMA	2019	Collaborative	-	250	400–2500	5–30	30	[111]

* Satellite decommissioned.

3.1.2. Aircraft

Aircraft address satellite limitations by offering higher resolutions, covering large areas at lower flight heights with superior spatial and radiometric resolutions [124]. However, similar to satellites, aircraft are sensitive to cloud cover and operational demands. Moreover, the use of aircraft requires specialized pilots, and factors such as geographic and atmospheric conditions may make them impractical, consequently leading to increased operational costs. Consequently, for smaller projects (up to a few hectares), aircraft use can prove financially unaffordable [124]. In olive growing, aircraft find application in irrigation management, water stress indicator estimation, ET and K_c estimation, biophysical parameter estimation and disease detection/monitoring. In some studies, aircraft were preferred for medium-scale study areas (400 to 3000 ha) and when sensor weight exceeded UAV capacity. For instance, the HSP sensor used by Berni et al. [125] and Calderón et al. [126] can weigh up to 5 kg, and the LiDAR sensor used by Estornell et al. [127] can weigh up to 100 kg.

3.1.3. Unmanned Aerial Vehicles

Over the past decade, the use of UAVs in PA has gained interest, offering high spatial/temporal resolutions, flexibility and reduced costs for small projects and for long-term monitoring [43,128]. UAVs bridge the gap between the large-area imagery of satellites and aircraft and the data accuracy of terrestrial techniques [129,130]. Depending on factors such as sensor type, spatial resolution, coverage area and intended application, the costs associated with using both platforms show variability, as analyzed by Pádua et al. [43]. There are two main UAV types, rotary-wing (RW) and fixed-wing (FW) [130,131], each with its advantages and disadvantages. RW UAVs can fly at lower flight heights, hover and perform low-speed flights, offering flexibility without specific take-off/landing requirements, which is crucial in some areas [131]. FW UAVs usually have the capability of longer flight durations, covering larger areas than RW UAVs but with lower image resolution [131]. A

technical comparison by Matese et al. [124] assessed cost-effectiveness, with UAVs as the most flexible, showing independence from cloud coverage and superior processing tasks. In small fields (~5 ha), RW UAVs were considered the most economical solution. Smaller FW UAVs could be used for up to a square kilometer (100 ha) with a spatial resolution from 0.05 m/pixel to 0.10 m/pixel. The extent of the area covered by a single image depends on flight height, speed, resistance and sensor resolution. UAVs, with high-resolution image sensors, offer precise data on large-scale crops and trees, even with minor cloud cover [132,133]. Due to UAV flexibility, this sensing platform finds extensive use in olive orchards, including inventory management, yield estimation, biophysical parameter estimation and disease detection/monitoring. Table 4 lists UAVs used in olive-growing applications.

Table 4. Unmanned aerial vehicles used in olive-growing applications from the identified studies. MSP: multispectral; HSP: hyperspectral; TIR: thermal infrared; N.S.: not specified or flexible depending on the study.

Wing Type	Model	Release Year	Maximum Payload (g)	Autonomy (min)	Sensors Used	Study References
Rotary	Microdones MD4-1000	2010	1200	45	RGB and MSP	[134–139]
	DJI S800	2012	2500	16	RGB	[33]
	DJI Phantom 2	2013	1300	25	RGB and TIR	[140]
	DJI S1000	2014	6000	15	RGB, MSP and TIR	[141–145]
	G4 Robot	2014	2300	28	RGB and MSP	[17]
	AscTec Falcon 8	2014	800	26	RGB and MSP	[146]
	ATyges FV-8	2014	1500	30	RGB and MSP	[146]
	DJI Matrice 100	2015	1000	40	RGB and MSP	[19,20,147,148]
	DJI Phantom 3	2015	1000	25	RGB and MSP	[149,150]
	DJI Phantom 4	2016	500	30	RGB and MSP	[19,22,151–167]
	DJI Matrice 600 Pro	2016	6000	38	RGB, MSP and HSP	[97,168,169]
	DJI Mavic Pro	2016	1200	21	RGB, MSP and HSP	[29,154,168,170,171]
	Mikrokopter MK8-2500	2016	2500	40	MSP and TIR	[172]
	Parrot Bluegrass	2017	1000	25	RGB and MSP	[173]
	DJI Matrice 210	2017	2300	38	RGB and MSP	[169,174]
	DJI Spark	2017	N.S.	16	RGB	[32,175]
	DJI Mavic Pro 2	2018	900	30	RGB and TIR	[28,155]
	DJI Mavic Air 2	2020	800	34	RGB	[176]
	Modified UAV	N.S.	N.S.	N.S.	RGB, MSP and TIR	[177–180]
Fixed	senseFly eBee	2013	800	50	MSP	[14,22,156,181–183]
	Parrot DiscoPro AG	2017	700	30	RGB	[153]
	Trinity F90+	2018	700	90	RGB and MSP	[184]

3.1.4. Terrestrial

Terrestrial equipment, such as terrestrial laser scanners (TLSs), characterized by its close proximity to the terrain, offers high-resolution data with excellent positional accuracy and enables in situ data classification. In agriculture, these tools can accurately delineate and provide 3D representations of crops, enabling precise dendrometric measurements from tree crown to trunk [43]. A study by Moorthy et al. [185] used an Intelligent Laser Ranging and Imaging System to construct and describe dimensional parameters of olive tree crowns, including foliar assemblage characteristics. However, these tools are not widely adopted in agriculture due to their labor-intensive and time-consuming nature, as well as their limitation of only providing line-of-sight observations [43]. Moreover, the use of equipment such as cranes, tractors, poles or even an operator crossing the field on foot can be indirectly classified as a terrestrial platform.

3.1.5. Summary

Understanding the trade-offs among key parameters, such as coverage area, spatial resolution, operational cost and deployability, is essential for optimizing the application of RS technologies in agricultural contexts. The absence of a universally optimal platform in RS applied to agriculture demands a discriminating evaluation of these factors. Table 5

provides a comparative and generic overview of the primary characteristics and limitations associated with the use of different RS platforms within the agricultural domain.

Table 5. Overview of the main characteristics of the different remote sensing platforms.

Performance Metrics	Satellite	Aircraft	UAV	Terrestrial
Coverage area	Worldwide	Regional	Local	Sub-Local
Spatial resolution	Low	Medium	High	Very high
Cloud sensitivity	High	High	Low	None
Deployability	Complex	Moderate	Low	Low
Availability	Low	Medium	High	High
Accuracy	Low	Medium	High	High

Satellites generally provide global coverage, making them suitable for large-scale agricultural monitoring at the district, province or even country level. However, their higher orbit flight height typically results in lower spatial resolution compared to other platforms. This trade-off directly affects the platform's capability to conduct detailed analyses at the individual crop level. Additionally, sensitivity to cloud cover introduces temporal constraints on satellite imagery availability, posing challenges during specific periods. Alternatively, aircraft, ideal for regional applications, offer a balance between coverage area and spatial resolution. Despite higher operational costs and moderate deployability, aircraft demonstrate versatility in diverse agricultural environments, particularly those requiring heavy payload support. They demonstrate flexibility against cloud cover, ensuring improved data availability. UAVs, with superior spatial resolution, surpass others in local-scale applications. Balancing lower operational costs with reduced susceptibility to cloud cover, UAVs have become a robust choice for reliable data acquisition. However, regulatory restrictions on flight operations significantly constrain this platform due to its extensive use in the past two decades. Terrestrial platforms, limited to local coverage, feature the highest spatial resolution, making them ideal for detailed research in specific areas within fields. Characterized by low operational costs and high deployability, these platforms outperform others in ground-level assessments; however, they face challenges in efficiently covering large agricultural areas.

3.2. Imaging Sensors

Imaging sensors, or sensing payloads, are crucial components of RS systems, capturing images without physical contact [43]. These sensors perform a crucial function in generating spatial information about the area of interest, enabling visual interpretation by identifying spatial relationships between objects. A diverse range of imaging sensors with varying spatial, temporal and spectral resolutions is available today. Each sensor can operate in different wavelengths of the electromagnetic spectrum, such as gamma rays, X-rays, ultraviolet light, visible light, infrared light, microwaves and radio waves [43].

In the domain of RS applied to agriculture, sensor selection is crucial, influencing the quality and applicability of data. This section presents critical considerations and several sensor types, offering insights into their applications in olive orchards. Choosing a specific sensor for RS agricultural applications demands a detailed evaluation of key characteristics [186]:

- Deployment platform: ground-based (e.g., terrestrial laser scanner), airborne (e.g., aircraft and UAVs) or spaceborne (e.g., satellites), significantly influencing data acquisition, considering orbit geometry, flight height and sensor compatibility.
- Wavelength spectrum: sensors operate across diverse wavelengths, including optical, infrared, thermal and microwave. This spectrum choice determines the type of information captured, impacting the utility of the data.
- Spatial Resolution: maintaining a balance between high and low spatial resolution is crucial, influencing the level of detail in the acquired data.

- Sensor type: choosing between narrow-band sensors (e.g., HSP) or broad-band sensors (mono and MSP) affects the sensor's ability to discriminate specific spectral features.
- Radiometric resolution: this feature delineates a sensor's capacity to differentiate between radiation levels, directly influencing the accuracy of the captured data.

The following sections briefly present the most common types of sensors used in RS, particularly in olive orchards, namely RGB sensors (visible light); MSP, HSP and TIR sensors; and LiDAR sensors (which can operate in both visible and infrared light).

3.2.1. Visible Light Sensors

Operating within the 400 to 700 nm wavelength range, visible light sensors capture images perceptible to the human eye. RGB sensors, with their composition of red, green and blue bands, are extensively used due to their cost-effectiveness and integration versatility. However, limitations exist regarding spectral information for tasks related to vegetation reflectance [43,187,188]. Additionally, through photogrammetric processing, these sensors can also provide digital elevation models (DEMs), primarily used for extracting object heights [43]. In olive growing, RGB sensors on board satellites and UAVs are primarily used (standalone) for detecting and inventorying olive trees. Typically, the information from these sensors is combined with data from other sensors, such as MSP data, and/or used for visual interpretation purposes.

3.2.2. Infrared Sensors

In the spectrum between 700 nm (near infrared—NIR) and 100,000 nm (far infrared), NIR sensors are crucial in RS applications for agriculture. Photosynthesizing plants, particularly in the NIR wavelength (which can be captured by MSP sensors), demonstrate significant reflection of incident sunlight [189]. This reflectance, which is sensitive to leaf cell structure, becomes key in assessing several agricultural parameters. Despite their higher cost compared to RGB, MSP sensors provide precise and consistent data applicable beyond basic detection and inventorying [43]. In olive orchards, these sensors are indispensable for assessing agro-environmental indicators such as K_c, managing irrigation and estimating crown dendrometric parameters. The data from MSP sensors are often combined with information from HSP or TIR sensors to improve disease detection, identify irrigated olive orchards, estimate water status indicators and evaluate ET_c [43].

HSP sensors represent a significant advancement in capturing imaging data. In contrast to MSP, HSP sensors capture information in narrow and contiguous spectral bands across a broader spectral range. This capability results in a detailed spectral signature for each pixel in the scene. Nevertheless, while these sensors offer a high spectral resolution, enabling the identification and quantification of molecular absorption, there are certain challenges. The high associated cost and the fact that most HSP sensors are line-array make them heavier and require specialized software. Consequently, common UAVs may lack the payload capacity for these sensors, requiring more robust UAVs for deployment [190]. In olive growing, HSP sensors find application in disease detection, especially for distinguishing variations in spectral signatures associated with specific diseases.

Operating in the electromagnetic spectrum between mid-to-FIR and microwave ranges (4 to 20 μm), TIR sensors are indispensable in agricultural monitoring. While more expensive than RGB sensors and usually offering lower image resolution, TIR imagery is useful in several applications. In the context of olive growing, TIR sensors demonstrated their effectiveness in irrigation management, estimation of water status indicators, ET_c assessment and disease detection [191]. TIR imagery is particularly useful for monitoring crop and soil conditions, including the estimation of water soil content and crop water stress for irrigation scheduling. Additionally, TIR sensors support the detection of diseases and pathogens and the mapping of soil texture. Despite their cost and resolution limitations, TIR sensors provide essential data for comprehensive agricultural analyses and management strategies in olive orchards.

3.2.3. LiDAR Sensors

LiDAR technology offers the capability for the three-dimensional scanning of various objects. Since the 1980s, LiDAR sensors have been extensively used in agricultural studies, applying principles such as time-of-flight (ToF), interferometry and triangulation [192]. In contrast to passive sensors, a LiDAR sensor is an active sensor that emits its energy source for illumination, allowing it to operate even at night. This technology enables a detailed geometric and radiometric representation of scanned objects. LiDAR sensors are used in two primary configurations: terrestrial laser scanner (TLS) and airborne laser scanner (ALS). While ALS provides broader coverage and higher point cloud density, TLS demonstrates advantages such as low-cost operation and easier multi-temporal data acquisition. In agricultural applications, these sensors, especially TLSs, are instrumental in estimating crop height for biomass calculation and growth monitoring [193]. In olive orchards, LiDAR technology has been successfully applied for the estimation of olive tree dendrometric parameters and wood volume.

3.2.4. Summary

In an increasingly diverse range of sensor types, understanding critical parameters such as spectral resolution, atmospheric interference, spatial precision and technological adaptability is essential for optimizing the effectiveness of RS methodologies across diverse fields. As verified in Section 3.1.5, with RS platforms, there is no universally optimal sensor type for all agronomical applications. The appropriate choice relies on the specific parameters and application context. Table 6 provides a comparative overview delineating the key attributes and limitations inherent to different sensors used in RS platforms, thereby supporting informed decision-making in selecting the most fitting sensor for customized applications.

Table 6. Overview of the main characteristics of the different remote sensing sensors.

Performance Metrics	RGB	MSP	TIR	HSP	LiDAR
Cost	Low	Medium	Medium	High	High
Operational principle	Passive	Passive	Passive	Passive	Active
Atmospheric interference	Minimal	Moderate	High	High	Minimal
Wavelength range (nm)	400–700	400–1000	8000–14,000	400–2500	905–1550
No. of bands	3	3–10	1	>100	N.A.
Band narrowness	Broad	Narrow	Broad	Very narrow	N.A.
Band structure	Discrete	Discrete	Discrete	Contiguous	N.A.
Pixel size	Small	Small–Moderate	Moderate–Large	Small–Moderate	N.A.

MSP: multispectral; TIR: thermal infrared; HSP: hyperspectral; N.A.: not applicable.

RGB sensors are widely used in simple agricultural monitoring tasks. These sensors are used for tasks such as visualization, inventory management and biophysical parameter estimation. Additionally, they are valuable for identifying visual symptoms in plants caused by diseases or pests [194]. When integrated into satellites, sensors sensitive to visible wavelengths occasionally produce panchromatic images with even higher spatial resolution than those generated by separate bands. Consequently, both panchromatic and RGB images in the visible spectrum are suitable for studies requiring detailed analysis [195].

In contrast, infrared sensors such as MSP sensors offer a broader spectral range than RGB sensors, allowing the analysis of vegetation health and crop characteristics. With moderate to high spatial resolution and the ability to capture data across multiple bands, they are essential for PA applications. VIs are the most common products used in multispectral RS for estimating various biophysical parameters. Additionally, some satellite-based spectral cameras, such as the Moderate Resolution Imaging Spectroradiometer (MODIS), capture more bands than standard multispectral cameras, providing improved capabilities [43]. Operating on higher wavelength ranges, TIR sensors, despite technological advancements, show lower resolution compared to RGB and MSP cameras. However, they

outperform others in identifying crop water stress conditions and detecting nutrient stress symptoms earlier than visible sensors [196]. These sensors can be cooled cameras, which provide direct measurements using quantum detectors cooled to cryogenic temperatures, while uncooled cameras rely on thermal detectors for indirect measurement [197]. Despite their lower spatial resolution and sensitivity, uncooled cameras are preferred for their affordability, compact size and operational convenience, especially for UAVs.

HSP sensors provide the highest level of spectral resolution among the discussed sensor types. With numerous contiguous narrow bands across a wide spectral range, HSP sensors enable detailed analysis of crop health, nutrient levels and soil composition. However, they are often more expensive and complex than MSP and RGB cameras, limiting their regular applications. Nevertheless, they offer detailed information about each band's reflectance in a wide spectral range, enabling the identification of the most informative bands for specific phenomena [198].

As the only active RS sensor discussed in this study, LiDAR sensors provide high spatial resolution and detailed 3D information about agricultural crops. Despite lacking spectral data capture, they are essential for terrain mapping and crop height measurement using a narrow bandwidth with high intensity and minimal divergence. Although theoretically operable in any wavelength, specific bands are chosen depending on the application, with emerging multispectral LiDAR sensors using multiple bands [199]. Despite their potential, multispectral LiDAR sensors are not yet fully operational, with single-band LiDAR sensors predominant in agricultural RS.

3.3. Data Type and Image Processing Techniques
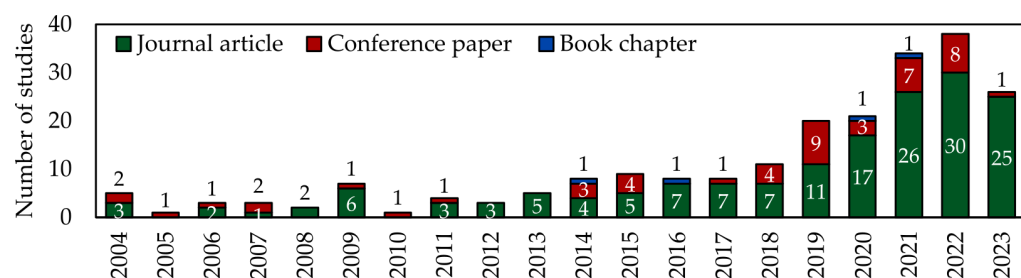
RS data obtained from UAVs and aircraft are essential in large-scale photogrammetric mapping [200,201]. Despite challenges such as platform stability and the use of non-metric cameras, photogrammetry remains attractive due to its higher spatial resolution, flexibility in acquisition timing and cost-effectiveness [202–205]. High-resolution digital images acquired by these platforms have largely replaced analog aerial photography, assisted by onboard navigation systems and ground control points (GCPs) for precise positioning [200]. Nevertheless, this type of imagery requires post-processing and orthorectification processes. The post-processing phase involves the generation of digital surface models (DSMs) through aerial triangulation and the subsequent creation of a point cloud from image pairs [201]. This process can also produce digital terrain models (DTMs) by filtering the dense point cloud or interpolating dispersed points [206]. The resulting DSMs and DTMs can be used for orthorectification, enabling direct measurements and mosaic creation [207]. Digital image processing techniques in agriculture often include pre-processing and pixel classification steps [208]. Vegetation detection relies on segmenting pixels into vegetation (crops, invasive plants and trees) and background (soil and infrastructures). Common segmentation technologies can rely on color indices or VIs, thresholding, ML and deep learning (DL). More information about ML and DL can be found in [209]. VIs, derived from arithmetic operations on different bands, are widely used in RS for extracting information related to water status, vegetative vigor, disease presence and biomass estimation [210]. In this context, Rasmussen et al. [211] evaluated VIs, including Excess Green (ExG) [212], Normalized Green Red Difference Index (NGRDI) [213], NDVI and Enhanced Normalized Difference Vegetation Index (ENDVI), derived from cameras mounted on UAVs. Their study addresses the importance of addressing factors such as stability under ambient light conditions and angular reflectance variation during sunny conditions when using VIs for quantifying crop responses to treatments. The authors also highlighted the significance of testing mosaic production software for bidirectional reflectance evaluation.

4. Results

4.1. Overview of Annual Distribution of the Research Studies

The introduction of RS imagery to olive-growing applications was first documented in 2004, generating an increasing interest in recent years (Figure 3). RS, supported by diverse

platforms such as satellites, UAVs, aircraft and ground-based systems, has progressed into a critical tool for monitoring and improving agricultural practices in the specialized field of olive growing. Over the past two decades, there has been an advancement in the quality and resolution of data captured by the sensors on board RS platforms, enabling a precise analysis of olive orchards. This technological progress, coupled with an increasing scientific focus on improving the management and monitoring of olive orchards, became particularly evident in 2019. During this period, the number of research studies in this domain doubled compared to previous years. In the following three years, there was a remarkable and exponential increase in scientific publications, reaching a peak in 2022 with 38 research studies conducted across numerous applications in the field of olive growing. Publications from 2023 were excluded from Figure 3 as, when the queries were performed (17 November 2023), there was not a complete overview of the entire year allowing a comprehensive conclusion on this topic. However, it is crucial to mention that this review also covers studies published throughout 2023.

Figure 3. Number of research studies using remote sensing imagery for olive-growing applications by year.
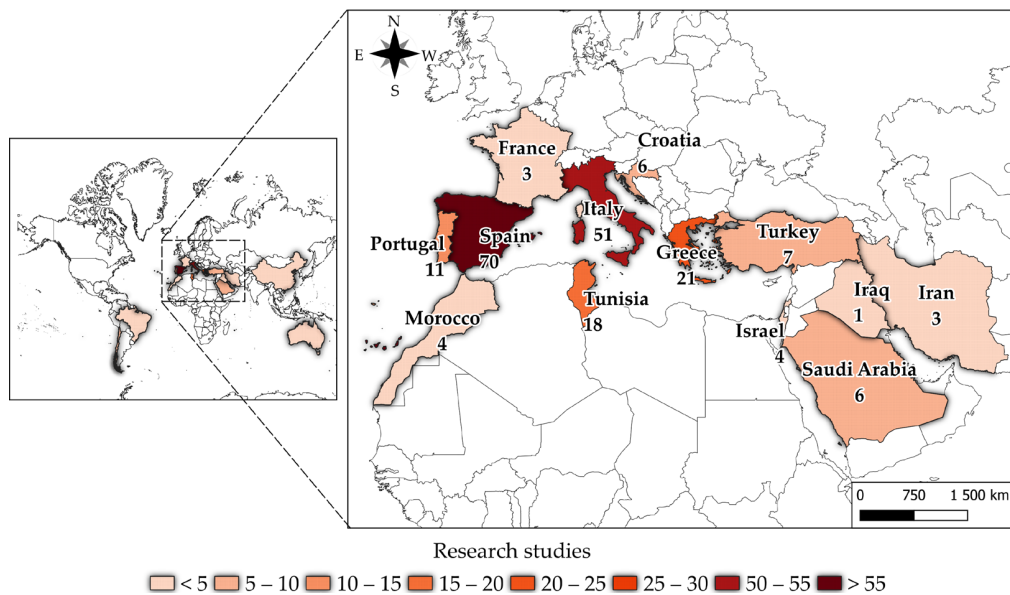
The diverse RS applications in olive growing have significantly contributed to operational efficiency, cost reduction and the mitigation of environmental impacts. In the future, the essential role of RS in the sustainable development of the olive sector is expected to persist. The integration of emerging technologies, such as DL and ML, stands as the promise of unveiling novel perspectives and further enhancing the efficacy and precision of RS applications within the olive-growing context.

4.2. Overview of Geographical Distribution of the Research Studies

The exploration of olive cultivation through RS imagery involves contributions from 17 countries. Despite this modest participation, a visible distribution across continents is evident, as illustrated in Figure 4. Regions such as Europe, North Africa, South America, Asia and Australia actively contribute to research studies related to olive growing. As expected, countries in the Mediterranean Basin and/or with a Mediterranean climate, known for their extensive olive cultivation practices, hold an important position in both production and harvested area, as outlined in Table 7.

A detailed analysis of scientific research, olive production quantity (t) and harvested area (ha) reveals discerning patterns (Table 7). Spain, the world's leading producer of olive oil, exceeds other countries in both scientific studies and olive cultivation metrics. Italy and Greece also show significance, presenting distinctions in production and harvested area. Countries such as Tunisia and Portugal, despite a substantial number of scientific studies, show comparatively smaller olive production and harvested areas than their European counterparts. Analyzing the production-to-harvested-area ratio reveals intriguing variations. Saudi Arabia stands out for its efficient production regarding its harvested area, suggesting effective agricultural management. In contrast, Israel and France present more conservative production concerning their harvested areas, suggesting potential areas for optimization in agricultural practices. The inclusion of diverse countries such as Iran, Iraq, Chile, Brazil and China in the analysis emphasizes the geographical diversity and varying scales of olive cultivation globally. This highlights the importance of considering

distinct regional contexts in comparative analyses. This critical examination reveals the complexities of the global olive landscape, emphasizing the need for contextual and integrated approaches when evaluating the application of RS and its implications for olive production worldwide.


Figure 4. Geographical distribution of research studies on remote sensing imagery in olive growing.
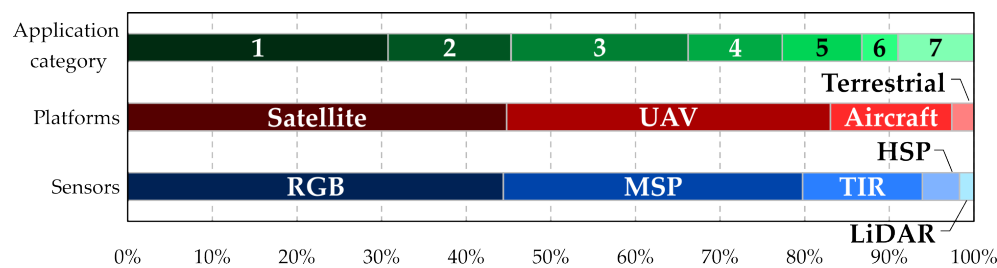
Table 7. Number of research studies using remote sensing data in olive growing, production quantity, area harvested and global contribution (data from FAOSTAT database 2021).

Country	Number of Studies	Production		Plantation Harvested	
		Quantity (t)	Global (%)	Area (ha)	Global (%)
Spain	70	8,256,550	35.1	2,623,290	25.4
Italy	51	2,270,630	9.7	1,129,000	10.9
Greece	21	3,045,100	13.0	826,390	8.0
Tunisia	18	700,000	3.0	1,251,313	12.1
Portugal	11	1,375,750	5.9	380,410	3.7
Chile	8	130,344	0.6	21,364	0.2
Turkey	7	1,738,680	7.4	889,168	8.6
Saudi Arabia	6	382,105	1.6	31,864	0.3
Croatia	6	23,870	0.1	19,940	0.2
Morocco	4	1,590,504	6.8	1,104,083	10.7
Israel	4	70,000	0.3	33,700	0.3
Australia	3	115,962	0.5	47,837	0.5
France	3	27,560	0.1	17,010	0.2
Iran	3	78,235	0.3	24,397	0.2
China	2	2619	0.01	315	0.003
Brazil	1	3417	0.01	2121	0.02
Iraq	1	33,314	0.1	8033	0.1

4.3. Overview of Technological Distribution of the Research Studies

The integration of RS applications in olive cultivation includes a diverse technological scenario, taking advantage of various platforms and sensors (Figure 5). In this context, satellites and UAVs emerge as predominant platforms, included in 47% and 40% of research studies, respectively. These platforms are crucial across multiple tasks, including inventory management, irrigation control, water stress estimation, biophysical parameter assessment and yield prediction. The distinct advantages of satellites, with extensive coverage, can be found in tasks related to ET and K_c estimation and phenology monitoring.

Conversely, UAVs present more usage in tasks such as biophysical assessments and disease detection/monitoring. The choice between these platforms depends on factors such as ground cover, spatial resolution and temporal information. Satellites provide large-scale temporal data crucial for phenology monitoring, while UAVs offer detailed spatial information, enabling individual tree monitoring, and are particularly valuable for the volumetric characterization of tree crowns. Aircraft, present in 15% of research studies, contribute to biophysical measurements, ET assessments, water stress indicator estimations and disease detection/monitoring. Equipping aircraft with HSP sensors improves their efficiency, especially considering weight considerations. In terms of sensors, RGB and MSP sensors emerge as the predominant choices, used in 84% and 67% of studies, respectively. RGB sensors find versatile applications, enhancing mosaic visualization, while MSP sensors, offering information across multiple spectral bands, contribute to diverse categories, including the estimation of biophysical parameters, yield assessments and inventory management. TIR, HSP and LiDAR sensors demonstrate comparatively lower usage, with their higher cost being one of the possible causes. TIR sensors, however, gain importance in irrigation management, water stress indicator estimations and ET assessments due to the correlation between crop temperature (T_c) and water stress. HSP sensors are useful for disease detection and monitoring due to their wide and selective electromagnetic spectrum range. LiDAR sensors show extreme precision in biophysical estimations.


Figure 5. Summary statistics of the technological distribution in the research studies analyzed per platform and sensor. UAV: unmanned aerial vehicle; MSP: multispectral; TIR: thermal infrared; HSP: hyperspectral. The application categories are as follows: 1—inventory; 2—irrigation management and water stress indicators; 3— biophysical parameters; 4—crop evapotranspiration and crop coefficients; 5—disease detection/monitoring; 6—yield; 7—others.
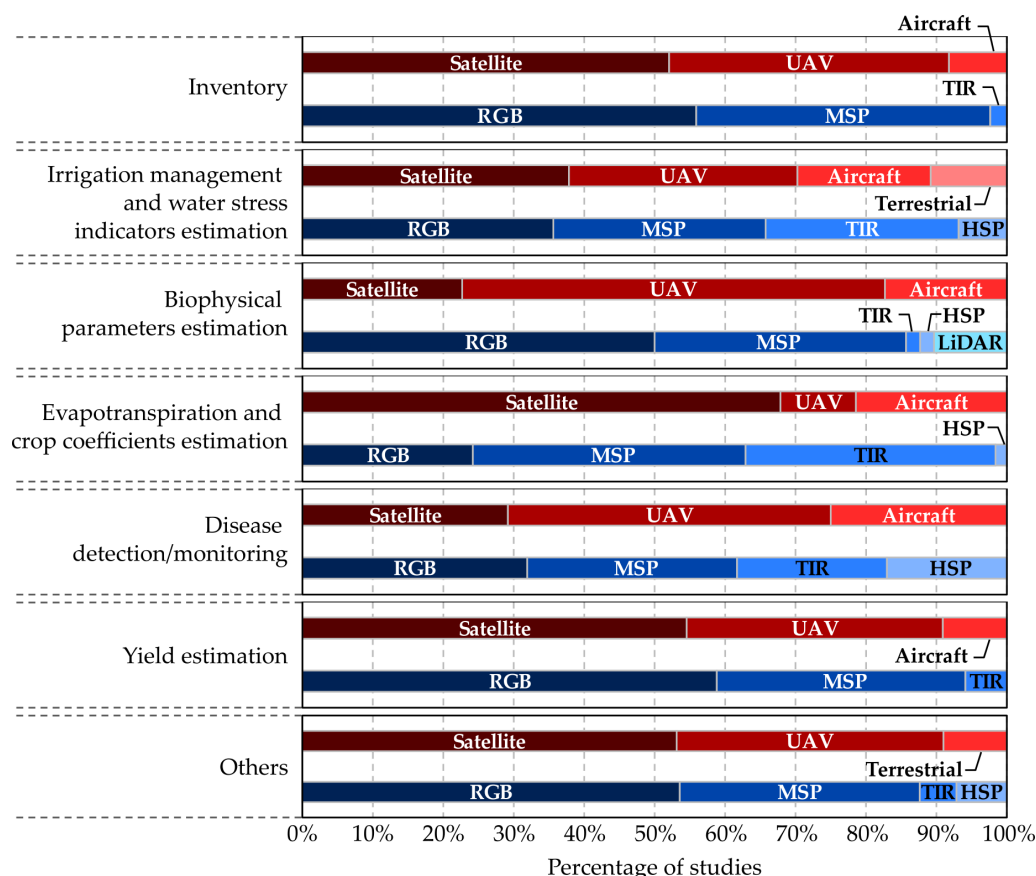
4.4. Remote Sensing Applications in Olive Growing

RS applications represent a classical and traditional approach extensively used in agriculture and agronomy for various purposes [8]. These applications include data acquisition and processing, establishing the basis for vegetation-related decision-making.

According to Salamí et al. [214], RS applications can be classified as passive, proactive or reactive based on their contribution to the process. Passive applications primarily focus on information acquisition, including inventory, dendrometric measurements, multi-temporal analysis of vegetation changes, modulation of biophysical and biochemical characteristics and mapping plant species [215,216]. In agriculture, passive applications can also monitor changes in crops over time to predict future growth [217]. In contrast, proactive applications include monitoring vegetation status to detect diseases, nutrient deficiency and invasive plants. Distinct from passive applications, proactive data acquisition is used for short-term decision-making [214]. This is commonly applied in PA, enabling precise estimation and application of fertilizers, pesticides, herbicides and irrigation based on specific crop needs in a particular area. In particular, monitoring water content in vegetation is crucial for optimizing irrigation strategies [130,217–219]. In olive growing, proactive applications have focused on disease detection, especially the detection of VW and *Xf*, which pose significant challenges in traditional olive orchards globally. The future potential for UAVs in reactive applications is expected to increase, enhancing their autonomous decision-making capabilities. In Japan, UAV-based systems are already applied for crop

spraying [188], considered a reactive application where sensor data are processed in real time and the system reacts based on verification results [214]. However, as reported by Zecha et al. [220], future advancements in such applications will require standardized data exchange and system components, addressing challenges such as the limited accuracy of position and orientation data, synchronization issues between image sensors and GPS navigation systems, variation between images, perspective distortion and variability in lighting conditions [221].

The following sections present an integrated analysis, emphasizing the strategic use of platforms and sensors in olive-growing applications, with a focus on platforms, sensors and outcomes. The distribution percentage of the RS platforms and sensors according to each application category is presented in Figure 6. Given the substantial volume of research studies in this review, only those published in scientific journals were selected for this detailed analysis. The sections are methodically organized based on predefined categories, where satellite platforms mainly contribute to broad-scale assessments, and UAVs, particularly those equipped with RGB and MSP sensors, are extensively used in tasks requiring detailed information.
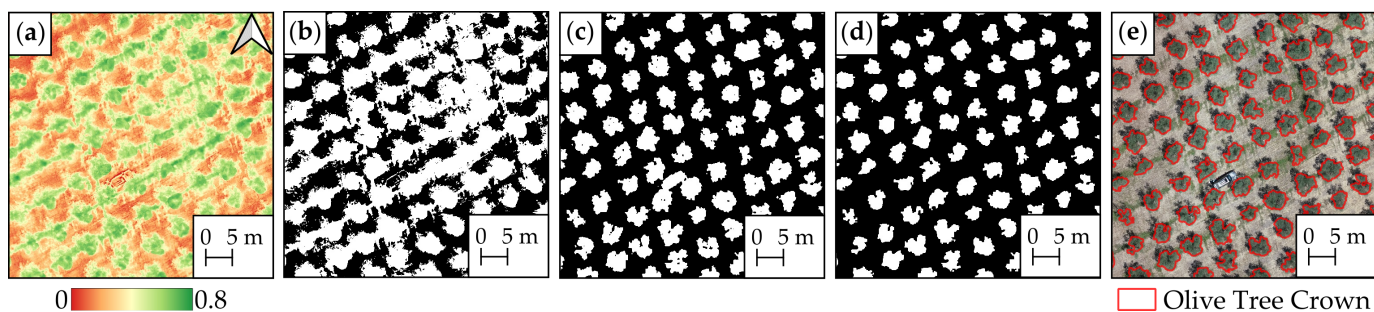

Figure 6. Summary statistics by application category. UAV: unmanned aerial vehicle; MSP: multi-spectral; TIR: thermal infrared; HSP: hyperspectral.

4.4.1. Inventory

In the context of inventory tasks in olive growing, satellites (52%) and UAVs (40%) represent the most common platforms used (Figure 6). This combined application reflects a strategic approach that influences the broad coverage offered by satellites and the detailed insights provided by UAVs. Within this context, RGB (56%) and MSP sensors (42%) represent the most common sensors used. The prominence of visual and MSP data underscores the significance of detailed color and spectral information in conducting detailed inventory assessments. To map olive trees effectively, numerous studies have explored diverse

platforms, sensors, segmentation methods and classification techniques in various olive orchards. Figure 7 shows an illustrative example regarding the detection and delineation of olive tree canopies using a threshold method applied to both the DEM and VIs from UAV-based data. This type of method represents a widely adopted approach in the literature; an example is presented in Figure 7. Initially, the NDVI is computed (Figure 7a), followed by the application of Otsu's method for thresholding (Figure 7b). However, the binarized image is composed of pixels from non-canopy olive trees due to low vegetation and other objects in the olive orchard. To address this issue, the canopy height model (CHM) is applied, considering only height values above 0.5 m (Figure 7c). Then, by merging the two previously binary images (Figure 7b,c), another image is generated (Figure 7d). This combination enables the identification and precise delineation of the olive tree canopies, as represented in Figure 7e.

Figure 7. Exemplification of the detection and delimitation of olive tree crowns: (**a**) Normalized Difference Vegetation Index (NDVI); (**b**) NDVI threshold; (**c**) canopy height model threshold; (**d**) combination of (**b,c**); (**e**) RGB orthophoto mosaic with the delimitation of olive tree crowns.

In the literature, also using UAVs, Torres-Sánchez et al. [134] recommended optimal configurations for 3D reconstruction, achieving around 95% accuracy. Karydas et al. [181] mapped orchards using an MSP sensor, reaching 93% overall accuracy. Beniaich et al. [150] used RGB imagery for color-based segmentation with an accuracy exceeding 99%. Jurado et al. [174] used 3D point clouds for detailed mapping, fusing photogrammetric point clouds and MSP data. Ye et al. [157] applied a DL approach (UAV-U2-Net) obtaining high precision (97.69% precision, 98.55% recall). Alshammari and Shahin [154] introduced Swin-TU-net, achieving 98.4% accuracy with low-cost sensors. Martínez-Ruedas et al. [222] classified orchard management systems with DL, presenting overall accuracies exceeding 0.8. Šiljeg et al. [169] compared ML models for olive tree crown extraction, where Geographic Object-Based Image Analysis–Support Vector Machine (GEOBIA-SVM) outperformed others. They also compared GEOBIA and VIs, with the Random Forest (RF) classifier showing the highest accuracy [184]. Yang et al. [158] explored OBIA-RF for crown outline extraction, achieving 96.5% accuracy. Lima-Cueto et al. [173] quantified vegetative ground cover with VIs, highlighting the importance of suitable algorithms and indices. Sarabia et al. [148] introduced a methodology for automated crop tree identification, demonstrating 99.67% accuracy. More information regarding OBIA, GEOBIA, RF and SVM can be found in [223–225].

However, different platforms, sensors and methods can be applied for the purpose of inventory. In particular, using Pleiades 1A satellite imagery, Alganci et al. [46] achieved 89% accuracy in estimating the spatial distribution and area of olive trees. Lin et al. [88] used WorldView-2, WorldView-3 and PlanetScope imagery, demonstrating 0.87 precision, 0.89 recall and 0.88 F1-score in semi-arid regions. Waleed et al. [226] addressed boundary issues with a high-pass filter and circular Hough transform, achieving a 1.27% overall estimation error. Khan et al. [227] introduced an automated method for olive tree counting using multi-level thresholding, achieving 96% overall accuracy. Castillejo-González et al. [82] assessed canopy delineation with pixel-based and object-based image analysis (OBIA), with Decision Tree (DT) [228] showing the highest overall accuracy (94.2%). Rivera et al. [98] compared unsupervised algorithms, and k-means clustering outperformed others.

Waleed et al. [229] performed olive tree detection with RGB images, concluding that RF was the most accurate (97.5%). Mezzi et al. [95] used Conditional Random Fields [230] for olive tree mapping, reaching a mean overall accuracy of 87%. Volpi et al. [109] developed a web-based tool for discriminating orchards, integrating NDVI patterns with 85% accuracy. Abozeid et al. [231] presented SwinTUnet, achieving 98.3% accuracy in olive tree detection, with challenges noted in dense areas. Martínez-Ruedas et al. [113] developed an automated methodology for inventory using Sentinel-2 imagery, characterizing 92% of Andalusian olive orchards. Martínez-Ruedas et al. [232] also validated a DL approach using convolutional neural networks (CNNs), achieving 95.7% accuracy for sub-images and 82.6% at the farm level.

Nevertheless, aircraft were also used for inventory purposes. Chemin and Beck [233] detected olive tree crowns using an aircraft and Leica RGB-infrared sensors, improving detection by 40% with the watershed method. Peña-Barragán et al. [234] employed an RGB sensor to assess cover crops, offering a cost-effective alternative to on-ground visits.

4.4.2. Irrigation Management and Water Stress Indicator Estimation
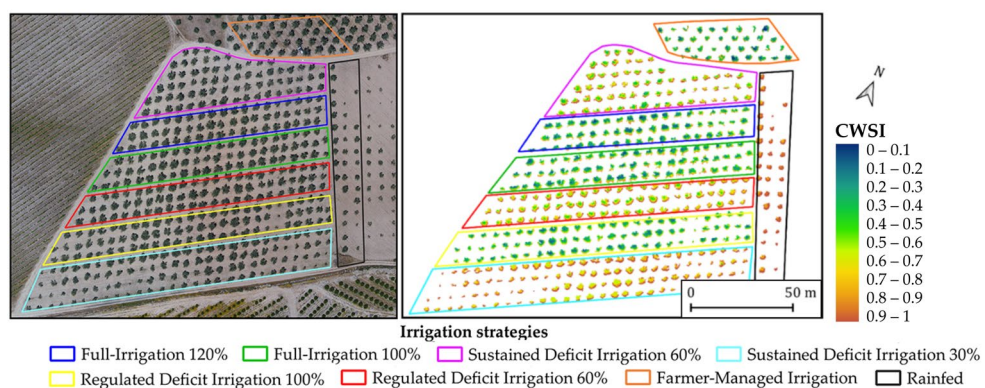
The investigation of irrigation management and the estimation of water stress indicators involved a diverse selection of platforms and sensors, as illustrated in Figure 6. Significant contributors to this field include satellites (38%) and UAVs (32%), with aircraft being used in 19% of the research studies. Furthermore, terrestrial platforms, such as imaging sensors placed above the canopy or readings conducted using a crane, were identified (11%). Regarding the sensors, a consistent usage pattern emerged among RGB (36%), MSP (30%) and TIR sensors (27%). While RGB images remain indispensable for visualization purposes, MSP and TIR images prove crucial for vegetation classification and T_c extraction, respectively. A modest use of HSP sensors (7%) was also observed in this category.

Using the Landsat 8 TIR and MSP data, Kefi et al. [92] performed a regional identification of irrigated and non-irrigated olive orchards. NDVI, Ratio Vegetation Index (RVI), Land Surface Temperature (LST) and Brightness Temperature (BT) characterized soil, while Vegetation Condition Index (VCI), Temperature Condition Index (TCI) and Vegetation Health Index (VHI) assessed stress conditions. NDVI indicated a higher vegetative vigor for irrigated orchards, and TIR data revealed stressed trees. Navrozidis et al. [104] developed a stress detection methodology with Sentinel-2 data, where quadratic discriminant analysis outperformed others. Sepulcre-Cantó et al. [235] used ASTER imagery to distinguish irrigated and rainfed orchards, achieving a 78% agreement. Chiraz et al. [112] assessed water productivity in different cultivation systems, revealing variations in productivity and efficiency.

In regard to the use of UAV platforms, Jorge et al. [152] used an MSP sensor to detect irrigation variations, finding strong correlations between NDVI and Green Normalized Difference Vegetation Index (GNDVI) [236]. Caruso et al. [143] assessed irrigation effects using both RGB and MSP sensors, highlighting significant water savings with minimal yield impact under deficit irrigation (DI). Santos-Rufo et al. [168] compared subsurface drip irrigation and surface drip irrigation impacts using RGB and HSP sensors coupled to UAVs. Different classification methods were used, highlighting the significance of wavelength ranges in detection. As for the estimation of water status indicators, Marques et al. [22] conducted an extensive evaluation of numerous spectral VIs and thermal data derived from UAV-acquired imagery for estimating water status indicators and leaf pigment content in olive trees under DI and full irrigation (FI) irrigation strategies. The results revealed that DI negatively impacted chlorophyll (Chl) and carotenoid levels, affecting spectral reflectance. Crop Water Stress Index (CWSI) [237] accurately predicted Relative Water Content (RWC), Stem Water Potential (Ψ_{MD}) and Stomatal Conductance (g_s) with R^2 = 0.80, 0.61 and 0.72, respectively. Modified Chlorophyll Absorption in Reflectance Index (MCARI) [238] estimated Chl_b (R^2 = 0.52), while Transformed Vegetation Index (TVI) [239] outperformed others in estimating Chl_a (R^2 = 0.61) and Chl_{ab} (R^2 = 0.64). All VIs presented

poor correlations with carotenoid estimation due to the absence of the blue spectrum. Egea et al. [140] correlated CWSI with water status indicators in super-high-density orchards.

Ben-Gal et al. [240] estimated soil and crop water status using analytical and empirical CWSI, showing high correlations with T_c. Berni et al. [130] investigated water status dynamics using a crane equipped with a TIR sensor, highlighting the effectiveness of empirical CWSIE in capturing water status dynamics. Noguera et al. [21] used a manually operated TIR sensor on a crane, revealing varied T_c responses between irrigation strategies. The authors suggested that DI-exposed olive trees showed higher T_c, particularly at 15 PM. However, correlations between water status indicators and T_c were lower at this time of day. Figure 8 shows an example of CWSI used for irrigation management and water stress estimation purposes.
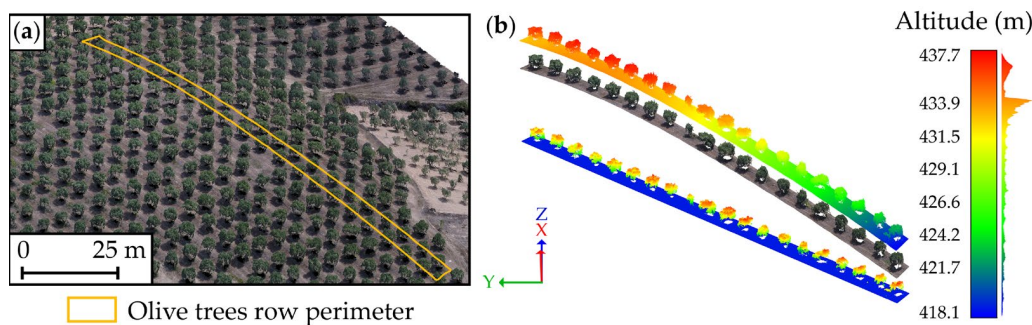
Figure 8. Example of the Crop Water Stress Index (CWSI) of an olive orchard (adapted from [156]).

4.4.3. Biophysical Parameter Estimation

Biophysical parameters, including biomass, crown dendrometry, LAI and Chl, represent crucial indicators for assessing the health status, growth and productivity of agricultural crops [100]. The timely availability of such data throughout a crop's life cycle not only supports farmers but also has proven invaluable for governmental institutions in making informed decisions. Through PA, driven by these biophysical metrics, farmers can implement targeted and sustainable practices, improving yield predictions and overall operational efficiency [102].
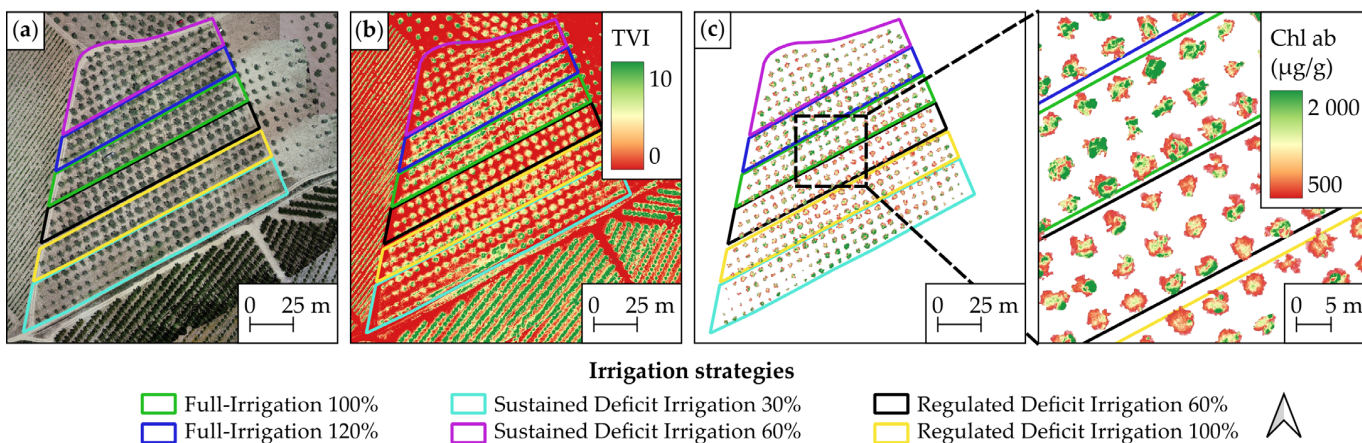
As observed in Section 4.4.1, approximately 85% of the studies in this field rely on satellite and UAV platforms equipped with RGB and MSP sensors, as illustrated in Figure 6. This indicates that, when estimating biophysical parameters, authors do not prioritize high-resolution images or sensors with higher spectral capabilities. Consequently, it is evident that, for this particular task, more cost-effective platforms and sensors are considered sufficient. Additionally, in studies that perform dendrometric measurements, DEMs stand out as the predominant data product, providing a critical component for estimating the height of olive trees. Figure 9 provides a visual representation, highlighting a segment of an olive tree row within a dense point cloud (Figure 9a) captured by a UAV in an olive orchard.

The corresponding elevation is presented using a false color representation (Figure 9b), complemented by the RGB representation of the same point cloud section. A demonstration of the normalized point cloud section is also presented, where the ground is highlighted in blue, while other colors show height values attributed exclusively to the olive trees. This enhancement not only improves interpretability but also supports the discrimination of specific features, particularly the contrast between the ground and the olive trees. For this particular case of dendrometric estimations, the use of LiDAR sensors was verified, constituting 10% of the research studies. This technology, while exceptionally precise, is relatively expensive, which is reflected in its limited adoption.

Figure 9. Elevation profile visualization of an olive tree row using a photogrammetric dense point cloud: (**a**) overview of the olive orchard; (**b**) isolated row with heights illustrated in false colors, along with the profile perspective of the isolated row section, and with normalized heights illustrated in false colors.

Moreover, in applications of this category, VIs are widely used, serving as a valuable correlation for the desired parameters. Figure 10 exemplifies the estimation of Chl in an olive orchard using UAV-captured imagery and TVI [22].

Figure 10. Estimation of Chl_{ab} using vegetation indices: (**a**) RGB imagery; (**b**) vegetation index TVI; (**c**) estimation of Chl_{ab} shown in false color, overlaid onto the RGB mosaic for improved visual representation. The Chl_{ab} estimation was carried out through the function $Y = 306.84 \times e^{(0.2077 \times TVI)}$ as mentioned in [22].

For this application category, only Gómez et al. [81] used a satellite platform to perform dendrometric measurements, using Quickbird imagery and an HSP sensor to evaluate tree crown characteristics, achieving R^2 values from 0.82 to 0.65 for crown area and varied R^2 values from 0.87 to 0.70 for olive crown volume. The HSP approach outperformed others in the estimation of Leaf Area Index (LAI) and olive crown transmittance, showing superior R^2 values ranging from 0.71 to 0.75. However, for the estimation of other parameters such as Chl, LAI and Fraction of Photosynthetically Active Radiation (fPAR), this platform found its applicability. Makhloufi et al. [100] used RGB and MSP data from Sentinel-2 to implement an artificial neural network (ANN) for inverting the Discrete Anisotropic Radiative Transfer (DART) model. The study aimed to estimate biophysical properties, including Chl, Equivalent Water Thickness (EWT) and LAI. The ANN effectively captured phenological stages, exhibiting a decrease in Chl_{ab} during summer-induced tree stress. Spatial analysis revealed consistent evolutions in biophysical parameters, outperforming traditional methods. Abdelmoula et al. [102] estimated biophysical variables (LAI, Chl, water content (Cw) and mesophyll structure (N)) using a 3D RTM and a spatially and temporally regularized Markov Chain Monte Carlo (MCMC) approach. The study suggested potential improvements in parameter retrieval by combining data from both Sentinel-2 and

Sentinel-3. Adjustments to the MCMC time-series inversion approach were proposed to address temporal dependencies during significant changes. Leolini et al. [105] evaluated different VIs for estimating fPAR at the pixel scale using Sentinel-2 imagery. The 3D rescaling methodology highlighted the contributions of woody and herbaceous parts, overcoming biases introduced by variations in canopy height. GEMI and MCARI2/OSAVI showed superior performance in estimating olive tree fPAR compared to NDVI, emphasizing the limitations of conventional satellite imagery in accurately assessing olive orchard dynamics.

In contrast to satellite usage, UAV application within this domain has demonstrated significantly greater effectiveness in estimating dendrometric parameters. Zarco-Tejada et al. [241] assessed the canopy height within a discontinuous olive tree canopy using DSMs. The results demonstrated high accuracy, with an RMSE of 35 cm, relative RMSE of 11.5% and R^2 of 0.83. Furthermore, an assessment of the spatial resolution of input images on DSMs revealed stable relationships within the range of 5 to 30 cm per pixel. However, relationships declined rapidly for input images with resolutions below 35 cm per pixel. In particular, when using imagery with a resolution of 30 cm per pixel, errors below 15% were consistently achieved in DSM generation. De Castro et al. [136] used the OBIA algorithm for olive identification, reaching superior performance in intensive orchards for crown parameters, achieving R^2 values of 0.63 for hedgerow area and 0.79 for intensive volume. Torres-Sánchez et al. [135] achieved an accuracy of over 96% in modeling single-tree fields and of 100% in tree-row fields using an OBIA approach with an MSP sensor on a UAV. The reported tree height estimation accuracy average errors ranged from 0.17 to 0.53 m. Crown volume R^2 values were 0.65 and 0.63 for 50 m and 100 m flight height images, respectively. Also using an OBIA algorithm, Rallo et al. [138] analyzed the utility of such a method for selecting promising olive genotypes in breeding programs. Trait values consistently exceeded 0.85 for all traits, achieving good results in crown volume. Díaz-Varela et al. [242] applied DEMs with a low-cost UAV equipped with RGB and color infrared sensors for estimating olive tree crown parameters. Genotype-averaged data demonstrated high linear fits, particularly in height estimation for hedgerow plantations (R^2 = ~0.9). Çoşlu and Sönmez [149] achieved 96% accuracy in individual tree detection using only an RGB sensor on board a UAV. The study reported high user and producer accuracy for single tree crown borders. Stateras and Kalivas [147] used MSP and RGB sensors to estimate geometrical characteristics, showing significant correlations between aerial and ground measurements, particularly for crown volume. Safonova et al. [153] applied a DL method (Mask R-CNN) to estimate olive tree biovolume using RGB and optical VIs at different spatial resolutions. The best crown segmentation performance (F1-score = 100%) was achieved with the RGB subset at 0.03 m spatial resolution.

Moreover, the predominant use of UAVs has demonstrated a significant effectiveness in providing a comprehensive understanding of dendrometric parameters essential for orchard management. Studies such as the one conducted by Anifantis et al. [175] show the utility of UAV photogrammetry and 3D modeling techniques in assessing tree row volume (TRV). Despite the tendency of the 3D modeling technique (TRV1) to underestimate crown volume in super-high-density olive orchards, its accuracy, low labor requirements and time efficiency make it a valuable tool, particularly for orchards with dense canopies. Furthermore, research into the impacts of pruning methods, as highlighted by Jiménez-Brenes et al. [137], revealed the efficacy of UAV imagery. Adapted pruning (AP) and traditional pruning (TP) significantly reduced crown volume, revealing the potential of UAVs in evaluating and optimizing pruning strategies for economic and environmental benefits. However, in addition to the widespread use of UAVs for directly estimating geometrical crown parameters, they have also been used for estimating parameters such as Chl and fPAR. Catania et al. [162] explored NDVI's effectiveness using multispectral data to evaluate the nutritional status, biometric characteristics and vegetative condition. Despite low NDVI values, strong correlations were verified with vegetative parameters and the prediction of productivity. Moreover, canopy volume demonstrated a strong relationship with canopy area and total cross-sectional area, emphasizing the interconnected

nature of vigor conditions. Guillén-Climent et al. [180] investigated modeling methods for estimating instantaneous fIPAR in olive canopies using an MSP sensor. The results indicated the Orchard Radiation Interception Model (ORIM) yielded better accuracy than the 3D Forest Light Interaction Model (FLIGHT) for simulating fIPAR from field-measured parameters in olive canopies. Zarco-Tejada et al. [243] explored the efficacy of VIs in estimating Chl_{ab} in open tree canopies using high-spatial-resolution HSP data from an aircraft. Strong correlations were verified, with MCARI/OSAVI showing the highest at $R^2 = 0.69$. The study emphasized the importance of modeling approaches considering spatial resolution and scene characteristics for stress mapping and crop chlorosis detection in open-canopy scenarios.

Regarding the use of LiDAR technology coupled in aircraft, Estornell et al. [244] used LiDAR data to quantify pruning residual biomass, achieving an R^2 of 0.88 for crown area. While challenges were verified in accurately estimating maximum and minimum crown heights, the study contributes to the understanding of the impact of pruning on olive trees. Moreover, Hadaś et al. [245] explored the detailed aspects of LiDAR data processing. The study focused on the importance of processing methodologies, highlighting the accuracy of parameters derived from dense LiDAR point cloud data, especially for tree and crown base heights. The exploration of different radius size settings and the application of the α shape algorithm led to complexities of tree geometric parameter estimation, offering insights into potential strategies for optimizing LiDAR data analysis in agricultural management.

The integration of platforms such as UAVs, satellites and LiDAR not only refines dendrometric parameter estimation and other crown-related parameters but also provides a complete approach to orchard management, ultimately contributing to sustainable and efficient olive cultivation practices.

4.4.4. Crop Evapotranspiration and Crop Coefficient Estimation

Estimating ET_c is essential in PA for optimizing irrigation and resource management. It provides farmers with information regarding crop water needs, enabling efficient water use and maximizing yields [51]. Technologies such as satellites, UAVs and aircraft provide critical data on variables such as LST and VIs. The predominant adoption of satellites (68%), in combination with MSP (39%) and TIR sensors (35%), highlights the most common strategy for ET and K_c estimation (Figure 6). This category shows a lower use of UAVs. This low usage can be attributed to their limited coverage area compared to satellites and aircraft. Moreover, an essential consideration in studies related to ET estimation is the use of data across a more extensive and consistent temporal extent, such as daily data over a week/month. This factor makes the use of satellite RS data more favorable.

Combining Landsat 5 TM and Landsat 7 ETM+ data, Paço et al. [50] investigated the computation of K_c using SIMDualKc and METRIC models (more information regarding METRIC models can be found in [246]). The strong correlation ($R^2 = 0.86$) between ET and K_c derived from both models shows their reliability and precision in estimating ET in the context of olive growing. This not only validates the models but also highlights their applicability for fine-tuned water management strategies. Exploring the impact of pixel size on METRIC model's estimation, Ramírez-Cuesta et al. [247] provided insights into the model's performance at different resolutions. While radiative net flux (Rn) and soil heat flux (G) demonstrated scale-insensitive behavior, sensible heat flux (H) showed variations at varying image scales. The study highlights the importance of considering spatial resolutions for accurate ET estimations. Pôças et al. [51] extended the application of the METRIC model to super-intensive olive orchards, revealing a robust correlation ($R^2 = 0.85$) between METRIC-derived ET and ground-based computations. Despite a slight overestimation of ET, the study emphasizes the model's potential, although with considerations for specific orchard settings. In a comparative analysis of empirical ET calculation methods, Bchir et al. [23] validated METRIC estimates against five different methods, demonstrating strong correlations (R^2 values: 0.85 to 0.99). Minor underestimations were verified when incorporating Landasat-8 satellite imagery, supporting the reliability of these methods

for olive orchards. Alternative models, such as the Shuttleworth–Wallace (SW) model, were explored by Elfarkh et al. [64], revealing their efficacy in mapping ET and optimizing agricultural water use. The results indicated a promising RMSE of 0.38 mm/h and a bias of −0.1 mm/h, highlighting the model's potential for providing precise estimates of orchard water requirements. Pieri et al. [54] reported a substantial improvement in the accuracy of actual ET estimation using the Spatial Enhancer of Vegetation Index Image Series (SEVIS). This improvement was particularly noticeable during critical periods, such as the summer dry period. Furthermore, Häusler et al. [55] and Ortega-Salazar et al. [65] analyzed Landsat 7 (ETM+) imagery and Radiative Surface Energy Balance (RSEB) models for estimating actual ET in fragmented olive orchards, revealing the utility of these models for irrigation management and stress conditions.

Using an aircraft as the main platform, Cammalleri et al. [248] observed that the Penman–Monteith approach outperformed FAO-56 in measuring daily K_c fluctuations based on meteorological conditions. Incorporating local information improved potential transpiration estimates, enabling the model to accurately represent transpiration dynamics throughout the irrigation season, including dry and wet periods. The modeled ET showed strong agreement with micrometeorological observations, achieving an overall accuracy of approximately 0.3 mm day^{-1}. In a subsequent investigation [249], the authors evaluated the DisALEXI [250] and TSEB-IC [251] approaches for ET prediction, revealing robust agreement with local weather station measurements. The modeled fluxes showed negligible differences, consistently below 10 W/m^{-2}, with spatial patterns aligning, except in areas with extreme vegetation cover. However, challenges were verified when using absolute surface–air temperature differences in TIR-based energy balance modeling. While both TSEB applications presented advancements, TSEB-IC required specific conditions and evaluation at larger scales, whereas DisALEXI performed well for the study area but required further testing for small-scale applications. Similarly, Minacapilli et al. [252] conducted a comparative analysis, comparing the soil–water–atmosphere plant (SWAP) model with two surface energy balance (SEB) models (TSEB and SEBAL). Both SEB models accurately characterized spatial ET patterns; however, their ET values were smaller than those from SWAP. The study highlighted the imperative need for additional research to determine the better-performing SEB model. The findings, based on a single RS acquisition, underscored the critical importance of validating results through a time series of acquisitions for robust ET assessments.

Using a UAV equipped with a TIR sensor, Riveros-Burgos et al. [253] conducted an evaluation of a model for estimating actual ET in a super-intensive drip-irrigated olive orchard, applying meteorological data. The authors concluded that the simulated values of Rn, H, G, latent heat (LE) and actual ET generally showed good agreement with ground-based measurements within the olive orchard. However, significant discrepancies were identified when the olive trees experienced moderate water stress. With a distinct approach, Ortega-Farías et al. [172] estimated incoming solar radiation (Rs), Rn, H, G and LE over a drip-irrigated olive orchard using an RSEB algorithm with MSP and TIR cameras mounted on a UAV. The results revealed differences between energy balance fluxes above the tree canopy and the soil surface among rows. The study shows the efficacy of this RS platform in providing detailed, high-resolution images (spatial resolution of 0.06 m), providing a valuable tool for assessing spatial variability in the partitioning of Rn into G, H and LE over heterogeneous orchards.

4.4.5. Disease Detection/Monitoring

The timely detection and monitoring of diseases such as *Xf* and *VW* in olive trees are extremely important for the sustainability of olive orchards. These phytosanitary issues pose substantial threats to the health of olive trees, resulting in substantial economic impacts for farmers. Rigorous monitoring not only enables knowledge of disease dynamics but also allows the adoption of targeted strategies for prevention and management [170]. As observed in Section 4.4.2, a diverse range of platforms and sensors has been used for the

detection and monitoring of olive tree diseases (Figure 6). UAVs represent the majority, used in 46% of these studies, while satellites and aircraft also show some applicability. Among the sensors used, in addition to the widely used RGB (32%) and MSP sensors (30%) for visualization and vegetation detection, TIR (21%) and HSP sensors (17%) have also been used. This category stands out for its heightened use of HSP sensors, underscoring the critical role of detailed spectral information in disease identification.

Using MODIS satellite data, Telesca et al. [76] analyzed temporal variability in ET as an indirect indicator of plant water status, specifically related to *Xf* infection. The study identified distinct seasonal cycles, with infected orchards showing a more pronounced six-month cycle aligned with *Xf* infectivity duration. Multifractal analysis revealed differences in ET dynamics, showing the impact of *Xf*-induced desiccation on tree behavior. Hornero et al. [99] focused on satellite-based VIs for monitoring *Xf* infection, highlighting the effectiveness of Atmospherically Resistant Vegetation Index (ARVI) [254] and Optimized Soil-Adjusted Vegetation Index (OSAVI) [255] in disease incidence accuracy. The results indicated that indices minimizing atmospheric and background effects achieved the best performance. Poblete et al. [89] conducted a comparative analysis of high-resolution WorldView-2 and WorldView-3 imagery against HSP and TIR datasets for detecting *Xf*- and VW-infected olive trees. The study showed successful disease detection with an overall accuracy range of 0.63–0.83. Incorporating thermal information, such as CWSI, improved prediction accuracy by 10–15%, emphasizing the role of high-resolution MSP data in disease identification.

Regarding the use of UAVs for disease detection, Di Nidio et al. [256] used TIR and MSP data for nearly real-time assessment of olive trees affected by olive quick decline syndrome (OQDS) induced by *Xf*. Despite challenges in segmentation, the hybrid approach achieved high performance in disease detection, emphasizing the potential of UAVs for real-time monitoring. Castrignanò et al. [29] classified Xf symptom severity on olive trees using a combination of geostatistics and linear discriminant analysis (LDA). The method demonstrated overall accuracy for asymptomatic and symptomatic trees, with better performance at initial and low severity levels. In contrast, for VW detection, Calderón et al. [196] used UAV-based MSP and TIR sensors. The study revealed optimal conditions for maximizing differences in canopy temperature at midday. Several VIs, including Photochemical Reflectance Index (PRI) [257] and NDVI, were correlated with physiological stress and structural damage caused by VW. TIR indices such as CWSI and pigment indices (Blue Green Pigment Index (BGI) and Blue Red Pigment Index (BRI) [258]) emerged as effective indicators for early VW detection. Mamalis et al. [31] evaluated YOLO models in UAV imagery for tree detection and health classification on olive trees infected by VW. The m640 model outperformed other evaluated methods (YOLOv5, YOLOv3 and YOLOv5m), showing suitability for real-time applications. Additionally, Iatrou et al. [181] explored the application of a plant-growth-enhancing formulation (PGEF) for managing VW in olive trees, revealing positive impacts on VW management. As for the use of DL models, Ksibi et al. [259] assessed the classification of olive leaf diseases based on a UAV imagery dataset. MobiRes-Net outperformed other models (ResNet50 and MobileNet), achieving the highest accuracy, F1-score and recall, showing superiority in classifying specific disease categories (*Aculus olearius*, Olive scab, Peacock spot and Healthy).

Using aircraft, Calderón et al. [126] aimed at early detection and classification of VW severity in olive orchards using HSP and TIR sensors. The automatic classification method, applying LDA and SVM, achieved higher overall accuracy, with LDA showing a superior performance at initial and low severity levels. Poblete et al. [40] achieved *Xf* detection accuracies using RGB and NIR spectral bands, with VIs related to pigment degradation and Chl, such as CRI700M, modified PRIM1, VOG2 and TCARI/OSAVI coupled with CWSI, demonstrating high accuracy. The study concluded that MSP and TIR sensors can effectively monitor large-scale Xf-infected areas when carefully selecting band sets based on spectral band sensitivity. In an ML multi-stage method applied to HSP and TIR imagery, Poblete et al. [30] differentiated infections caused by VW and Xf. Spectral traits such as the

blue index B and carotenoid pigment content Cx + c were identified as key differentiators, demonstrating improved discrimination accuracy in sensitivity tests.

These studies show the importance of RS technologies, ranging from satellites to UAVs and aircraft, in disease detection and monitoring in olive orchards. The integration of MSP, HSP and TIR data, coupled with advanced image analysis techniques and ML models, provides an extensive and effective approach for identifying and managing diseases such as Xf and VW.

4.4.6. Yield Estimation

Crop yield prediction has generated significant attention within the research community and agricultural organizations. Precise yield prediction is extremely important for farmers, enabling them to improve fruit quality while simultaneously reducing operational costs. This is achieved through informed decision-making regarding the optimal intensity of fruit thinning and the appropriate resources for harvest operations [260]. With consistent trends, as observed in Sections 4.4.1 and 4.4.6, studies dedicated to predicting olive production predominantly focus on RGB and MSP data acquired from satellites or UAVs, accounting for over 90% of the total studies (Figure 6). This reaffirms the concept that opting for more cost-effective and readily available equipment proves sufficient for fulfilling this objective.

The methodologies proposed in this category, incorporating kNN segmentation and k-means clustering [32], Clustering Assessment® (CLUAS) software [80], CNN [34] and linear regression [33], reveal advancements in automated processes for data extraction and analysis in this field. García Torres et al. [80] and U. Khan et al. [34] used the Quickbird satellite for olive tree detection and yield estimation. Although these studies achieved high accuracy (95%) in olive tree detection and yield estimation, promising efficient orchard management, the authors acknowledged uncertainties in interpretation due to the low resolution of the imagery. Despite the higher spatial resolution (30–50 cm) of QuickBird satellite imagery in comparison to other satellites, it remains inferior to the resolutions achieved by UAVs (approximately 5 cm). Thus, when research intends to estimate the yield, such disparities in spatial resolutions may misrepresent the outcomes. Brilli et al. [77], using Landsat ETM+ and MODIS satellites, introduced a novel multi-step methodology for estimating gross primary productivity (GPP) in olive orchards. While the study emphasized the potential enhancement of the model with high-resolution satellite data, the modified C-Fix parametric model successfully simulated daily GPP, with discrepancies noted during post-tillage periods.

For the same purpose, several authors opted for higher spatial resolution images provided by UAVs [32,33,142], performing distinct approaches. Caruso et al. [142] focused on canopy variations and correlating spectral features with fruit yield. The study provided satisfactory estimations of canopy characteristics and introduced an innovative method for pruning material estimation. A positive linear relationship between NDVI and fruit yield was established, enhancing the understanding of orchard dynamics. Ortenzi et al. [32] investigated early yield estimation (during the flowering phase) using the canopy radius. The approach proved effective, providing a robust and reliable estimate of total production, with deviations from real values within acceptable limits. On the other hand, Sola-Guirado et al. [33] used olive tree crown volume and area for correlation with annual yield across various orchard categories, excluding super-high-density ones. The results revealed satisfactory correlations between tree crown characteristics and annual yield, offering flexibility in making predictions using either manual canopy volume or individual crown area. Despite minor variations among orchard categories in overall annual yield, the findings underscore the critical importance of optimizing canopy volume per hectare to mitigate yield gaps and improve harvesting efficiency. However, the authors emphasize that these relationships are context-specific, specifically to southern Spain, requiring adjustment coefficients for application in different regions. Additionally, the research identifies irrigation as an
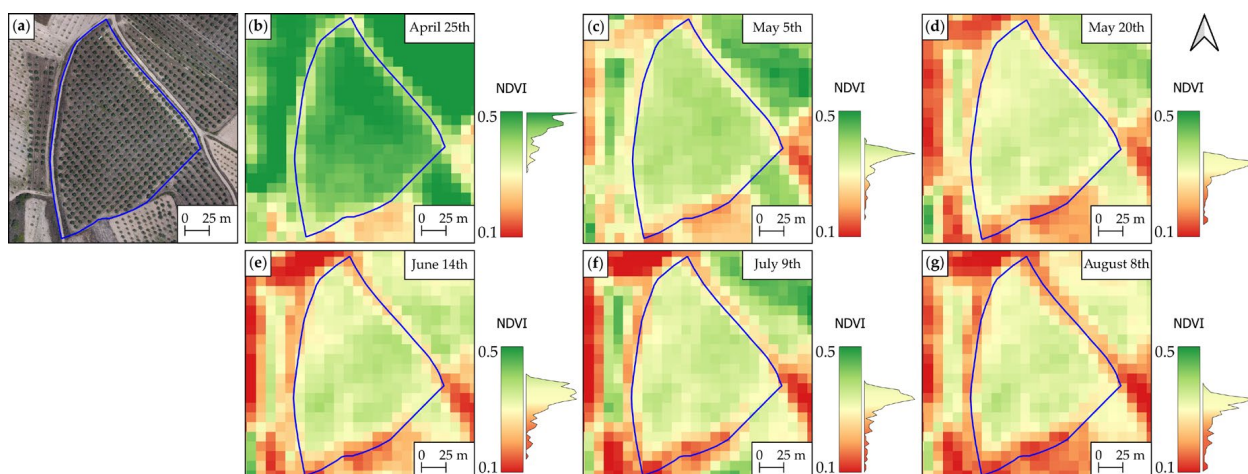
essential factor influencing annual yield, further emphasizing its significance in the olive orchard context.

In summary, while the choice of platforms varied, all studies demonstrated the efficacy of RS in improving orchard management. However, challenges such as misinterpretation uncertainties and spatial resolution limitations were acknowledged in some studies, indicating areas for future improvement.

4.4.7. Others

This category includes studies that use RS techniques for tasks such as phenology monitoring, landslide evolution, soil monitoring and fertilization monitoring. Depending on the specific task, different combinations of platforms and sensors were observed. However, the predominant approach involves using RGB and MSP data from satellites or UAVs, constituting the majority of studies (approximately 90%), as illustrated in Figure 6.

Accurate monitoring of crop development patterns, including phenology and growth, holds significant importance in farm management. It enables the assessment of whether crucial growth stages align with favorable weather conditions. Additionally, phenological monitoring improves knowledge of the intricate processes involved in crop development and growth [261]. Figure 11 illustrates a graphical representation of the influence of different phenological stages in an olive orchard on the temporal trends of NDVI values. Clearly, a decline in NDVI values is evident as the phenological stages develop. The establishment of correlations between these variables through such products enables the identification and monitoring of phenological states. This information is critical for guiding targeted interventions in the field.


Figure 11. Temporal surveying of olive orchard phenological states using satellite NDVI: (**a**) RGB imagery captured by UAV; (**b**) Leaf BBCH stage: 11, Inflorescence BBCH stage: 51; (**c**) Leaf BBCH stage: 11, Inflorescence BBCH stage: 54; (**d**) Leaf BBCH stage: 19, Inflorescence BBCH stage: 57; (**e**) Leaf BBCH stage: 19, Flowering BBCH stage: 68; (**f**) Leaf BBCH stage: 11, Fruit BBCH stage: 71; (**g**) Leaf BBCH stage: 11, Fruit BBCH stage: 75. The chart next to the legend represents the histogram of values within the orchard.

Azpiroz et al. [261] used ML methods to predict olive phenology in MODIS satellite imagery, incorporating climate reanalysis data. Numerous feature-selection techniques, including filtering and embedded methods, were used to assess the impact of different feature sets on prediction, aiming to simplify model complexity through a reduction in input variables. Recursive Feature Addition (RFA) emerged as the method with optimal performance without compromising accuracy. Among ML models, RF and extra tree regression proved the most efficient, with extra tree regression demonstrating the most accurate predictions. The model demonstrated adaptability across locations, maintaining accuracy even without geographic variables. The inclusion of precipitation, temperature

and features from climate data and VIs improved accuracy. Guermazi et al. [108] used RGB and MSP data from Sentinel-2A to determine olive tree phenological stages. Using time-series VIs, the research observed changes in Chl content, which is crucial for assessing olive phenology. The TCARI/OSAVI index effectively distinguished growth stages, revealing significant differences between rainfed and irrigated fields. Additionally, CIgreen emerged as the VI with the best performance in estimating Chl content variability. However, the authors suggest that the method is more suitable for arid and semi-arid regions like the Mediterranean, where olive trees are traditionally rainfed.

Using the HidroMORE model to spatially assess the impact of drought on olive orchards in southern Tunisia, Sghaier et al. [262] developed a decision support system with RS data and on-site measurements. The study demonstrated its reliability in mapping drought stress in diverse conditions, offering a scalable approach for wider applications. Emphasizing the effectiveness of traditional water harvesting systems and the significance of soil type selection, the findings provide an objective tool for prioritizing interventions during extended drought. Shaik et al. [111] explored the relationship between tree canopy temperature, canopy height and vegetation types in the Monte-Arcosu Forest of southern Sardinia Island. Canopy heights were estimated using an RF regression model with an R^2 = 0.79. Land use and land cover types were mapped using an SVM classifier with over 80% accuracy for each class. Furthermore, the authors observed a negative correlation between canopy height and T_c for several vegetation types. For a distinct purpose, Castelli et al. [66] used Landsat-7 imagery to assess the effectiveness of the jessour system in olive tree cultivation by comparing Normalized Difference Infrared Index (NDII) values in jessour and non-jessour sites, where high correlation were verified (R^2 between 0.62 and 0.67) throughout the year. Despite differences in soil characteristics, the linear relationship between NDII and soil moisture demonstrated the potential of NDII as a reliable indicator.

UAV-based imagery was also used for several distinct applications in olive orchards. Specifically, olive orchard soil characteristics were assessed by Dindaroğlu et al. [114] using ML methods on UAV and Sentinel-2A imagery. Positive correlations between VIs from UAV and Sentinel-2A data were observed. MLP models based on both UAV and Sentinel-2A demonstrated similar accuracy in estimating soil properties, with Gradient Descent Boosting Tree (GDBT) performing comparably to MLP in the Sentinel dataset. The authors recommend the fusion of Sentinel-2 and UAV images for reliable digital soil mapping, using both datasets for enhanced predictive modeling. Beniaich et al. [150] presented a novel UAV-based methodology for soil erosion monitoring. Using low-cost cameras and the RF classification algorithm, the study achieved accurate vegetation and bare soil classification (93% and 91%, respectively). The intercropping of olive plantations with spontaneous vegetation effectively controlled water erosion. Total Cover Index (TCI) proved a reliable predictor of soil loss and C-factor determination. The combination of TCI and erosivity demonstrated the best predictive performance, highlighting correlations between rainfall erosivity and C-factor. With a similar purpose, Fernández et al. [167] analyzed the erosion processes in a 16-hectare active gully. GIS analysis revealed gully area and perimeter increases, with bank line point displacement and surface changes indicating evolution mechanisms. In a distinct application, Fernández et al. [146] used DEMs retrieved from UAV imagery for a multi-temporal analysis of an earth flow affecting an olive orchard. The results enabled the characterization of slope movement flow rate and morphological features on a hillslope. The technique allowed multi-temporal analysis, measuring vertical displacements and identifying depletion and accumulation areas inside the landslide with an accuracy of about 0.10 m in XY and 0.15 m in Z. Furthermore, UAV imagery was also used for monitoring fertilization in olive orchards. In this context, Roma et al. [163] developed a GIS-based methodology for generating precision fertilizer prescription maps in olive orchards, addressing significant spatial variability in soil variables. UAV-based imagery allowed the analysis of vegetative vigor variability, resulting in a 31% reduction in fertilizer use compared to standard doses. This approach promoted economic, agronomic and environmental benefits, including sustainability and cost reduction. Similarly, Noguera
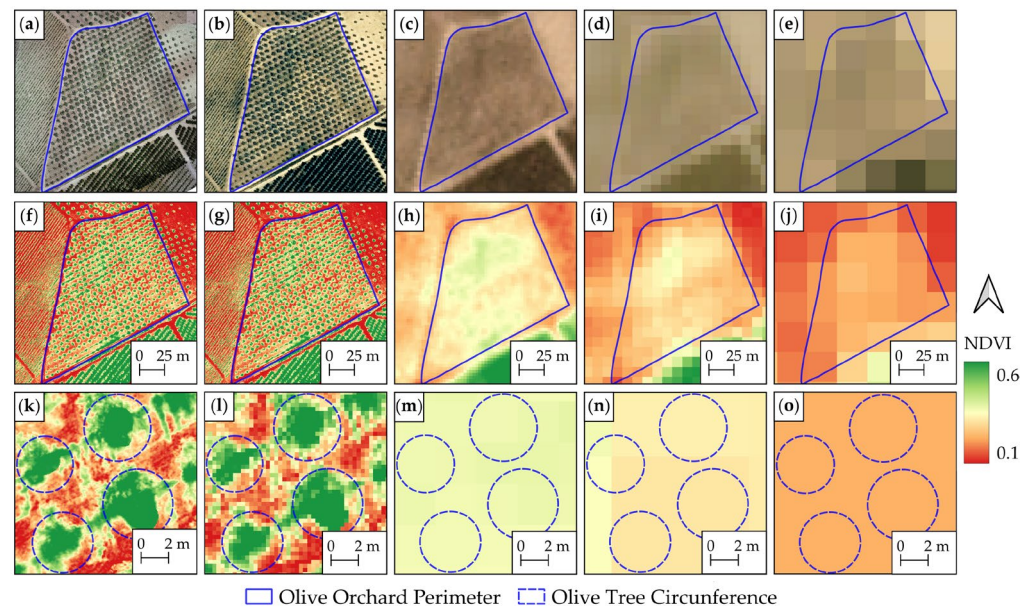
et al. [20] developed a method for assessing nitrogen, phosphorus and potassium foliar content in olive trees using MSP imagery acquired from a UAV. The image processing technique with an ANN proved to be optimal for nutrient content retrieval under field conditions. The method is capable of continuous assessment of olive orchard nutrient status, potentially optimizing fertilizer use and improving productivity and profitability in the olive sector.

4.5. Limitations and Future Perspectives

In the exploration of RS technologies applied to olive orchards, several limitations have emerged, offering valuable insights into the challenges faced by different RS platforms. These limitations included various aspects, including satellite imagery resolution, timing constraints and challenges associated with LiDAR and UAVs. Additionally, the estimation of critical parameters such as CWSI faces drawbacks, delaying the unified integration of RS into olive orchard management.

Satellite imagery, despite its widespread use, deals with intrinsic limitations. The coarser spatial resolutions, such as the resolution from Sentinel-2 (10 m GSD) and others with 1 km/pixel resolution, pose limitations to individual tree analysis. This issue, highlighted by Weissteiner et al. [263], Akcay et al. [47] and Alganci et al. [46], compromises the accuracy of identifying individual trees due to mixed information. A graphical representation illustrating this limitation is presented in Figure 12, where visual representations and NDVI maps of an olive orchard with approximately 1.5 ha are shown at different spatial resolutions (0.05 m from a UAV, 0.30 m from an aircraft, 3 m from PlanetScope, 10 m from Sentinel-2 and 30 m from Landsat 8). The visual distinctions between the data are easily observable. Regarding olive orchard perimeter identification, images with a spatial resolution inferior to 3 m proved to be visually informative (Figure 12a–c,f–h). However, for the individual identification of olive trees, a clear olive tree crown is evident only in data with a spatial resolution inferior to 0.3 m (Figure 12k,l). This outcome was expected in this specific scenario, given the olive trees in the example have a crown diameter of less than 3 m. Moreover, in raster products with a spatial resolution exceeding 10 m, a single pixel includes multiple olive trees. Specifically, at 30 m spatial resolution (Figure 12o), all four olive trees are contained within the same pixel. The distinctions among the various spatial resolutions are also easily visible in the pixel count of the olive orchard area: 70 million, 166,000, 1665, 151 and 17 for data from UAV, aircraft, PlanetScope, Sentinel-2 and Landsat 8, respectively. Regarding the mean pixel count per olive tree crown, the values are 78,000, 25,000, 1.8, 0.17 and 0.02 for raster products from UAV, aircraft, PlanetScope, Sentinel-2 and Landsat 8, respectively. These disparities across different spatial resolutions are also visible in the NDVI values. A visible pattern emerges: the lower spatial resolution, the lower the maximum NDVI values. This effect is clearly observed at the upper section of the olive orchard, where NDVI values are lower in coarser resolutions.

Moreover, temporal constraints associated with satellite overpasses, as stated by Ortega-Farías et al. [61] and Fuentes-Peñailillo et al. [62], result in incomplete datasets due to cloudiness and system noise. This limitation constrains the reliability of field measurements and assessments, impacting the overall efficacy of satellite-based monitoring. Furthermore, Sentinel-2A and B satellites, while providing valuable data, face challenges in determining phenological stages and accurately classifying orchards. Guermazi et al. [108] faced difficulties in capturing phenological changes due to local cloudiness, which limited the effectiveness of medium-spatial-resolution imagery in specific orchard types. Abubakar et al. [15] reported classification challenges, particularly in young orchards and heterogeneous plots. The interference arising from sparse canopies and age differences in trees underscores the need for improved classification methodologies customized for diverse orchard conditions.

Figure 12. RGB and NDVI maps of olive orchard area and olive tree crown acquired with different platforms and spatial resolutions: (**a**,**f**,**k**) from a UAV with 0.05 m; (**b**,**g**,**l**) aircraft with 0.30 m; (**c**,**h**,**m**) PlanetScope with 3 m; (**d**,**i**,**n**) Sentinel-2 with 10 m; (**e**,**j**,**o**) Landsat 8 with 30 m.

LiDAR sensors and UAV technologies, crucial for high-resolution data acquisition, also showed limitations. Estornell et al. [127] and Hadas et al. [264] highlighted errors in estimating dendrometric parameters, attributing them to low-density data and the absence of GCPs. This limitation underscores the importance of meticulous data collection and validation processes. UAV imagery encounters challenges in estimating diameter at breast height (DBH) in areas with high tree density, as reported by Moreira et al. [166]. The dense canopy obscures trunk images, affecting the accuracy of DBH estimation and calling for improved methodologies to address this limitation.

The estimation of CWSI emerges as a common challenge across RS platforms. Agam et al. [265] identified uncertainties related to the empirical value of 5 °C and the need for a wet reference in every flight campaign, limiting the frequency of data acquisition for stress monitoring. Egea et al. [140] further reported that the non-water-stressed baseline (NWSB) for CWSI calculation in super-high-density olive orchards is not constant throughout the growing season, complicating stress assessments.

Despite these limitations, the path of RS in olive orchard applications shows promising trends for the future. Continuous advancements in satellite technology, with the launch of high-resolution imaging satellites, are anticipated to address the spatial resolution challenges. Improved revisit times and enhanced capabilities for cloud penetration will contribute to more comprehensive and frequent data acquisition. The integration of AI and ML algorithms, especially DL, is expected to revolutionize feature extraction and classification processes. This will mitigate challenges related to tree detection, canopy delineation and classification accuracy in diverse orchard scenarios. Regarding the use of LiDAR in UAVs, increased data density and advancements in data processing algorithms will enhance the precision of dendrometric parameter estimation. Overcoming limitations in DBH estimation under dense canopies will be a focal point, with the integration of complementary technologies such as CHMs and improved image registration techniques.

Moreover, the future of RS in olive orchards is predicted to include the development of innovative methodologies for stress monitoring. Integration with ground-based sensing, IoT devices and improved models for CWSI calculation will provide more accurate and real-time insights into the water stress conditions of olive trees. As RS technologies continue to develop, collaborative efforts between researchers, technologists and agricultural

practitioners will be important in overcoming existing limitations and unlocking the full potential of RS for sustainable and efficient olive orchard management.

5. Conclusions

In the extensive exploration of RS applications in olive cultivation, this review analyzed studies from around the world, revealing the numerous benefits and diverse methodologies used. The versatility of RS platforms, from satellites and UAVs to aircraft and ground equipment, was a central theme of this article. As exposed in Section 3, the correct choice of a platform is crucial for the intended scope of the study, with satellites proving effective for large-scale district-level analyses due to their extensive coverage. However, if the size of the study area is relatively small or local, the use of UAVs will be the most suitable due to their high spatial resolution and costs. Concerning the type of sensors that can be used, as verified in the platforms, it also depends on the objective of the study and the type of data. If an analysis of crop water status indicators is intended to be carried out, the use of TIR sensors is recommended. However, if the objective is to detect and count the number of trees, RGB sensors are the most viable solution in terms of cost–benefit. Regarding the distribution of studies by countries, these studies were carried out in countries with a tradition in olive oil production, such as Spain, Italy, Greece, Tunisia, Turkey and Portugal, with emphasis on Spain, where 32% of the studies were carried out.

Case studies related to the use of RS in olive growing, the main theme of this manuscript, are presented in Section 4, with a critical analysis. In this area, the main applications are as follows: inventory, irrigation management and water stress indicator estimation, biophysical parameter estimation, ET and K_c estimation, disease detection/monitoring, yield estimation, phenology monitoring and others. The majority of the studies (30%) developed applications related to olive orchard inventory, i.e., detection and counting of the number of olive trees. Regarding the type of platform used, the majority of the studies used aerial images obtained by satellite (47%) and UAV (40%). However, it is expected that the use of UAVs will increase due to their increasingly reduced price due to the evolution of this technology and its advantages when compared to satellites [188]. Only 15% of the studies used aircraft, mainly due to the high cost associated with this technology [43,124]. As expected, RGB and MSP sensors are widely used (84% and 66% of the studies) since they are cost-effective and operate in the infrared spectrum, thus including the zone where the vegetation has high reflectance, in the NIR.

As evidenced by this review, despite the numerous works focusing on RS applications in olive growing, there is a noticeable lack of established techniques and frameworks that are reproducible and applicable across diverse conditions. The accuracy of RS data analysis methods depends on factors such as image resolution, atmospheric conditions and crop characteristics, resulting in uncertainties in decision-making processes [248].

Regarding trends and future perspectives in this field of application, there is no doubt that areas such as computing science, platforms and sensors will significantly be influenced by universal development trends. Advanced information and communication technologies, as well as spectral decomposition methods, will be a key factor in synthesizing data effectively and generating practical information crucial for PA applications. Artificial intelligence techniques hold considerable promise in generating spatially and temporally continuous information from RS data, addressing various PA needs. Hybrid approaches, integrating AI with knowledge from physically based models, will further enhance PA decision-making processes.

While challenges persist, there are opportunities to overcome them through technological advancements and interdisciplinary collaborations. Improvements in RS platforms, sensors, and data analysis techniques hold the potential to revolutionize olive cultivation practices, leading to more sustainable and efficient agricultural operations.

References

1. FAO. *The Future of Food and Agriculture: Trends and Challenges*; FAO: Rome, Italy, 2017; ISBN 978-92-5-109551-5.
2. Alexandratos, N.; Bruinsma, J. *World Agriculture towards 2030/2050: The 2012 Revision*; ESA Working Paper No. 12-03; FAO: Rome, Italy, 2012.
3. Sivakumar, M.V.K.; Gommes, R.; Baier, W. Agrometeorology and Sustainable Agriculture. *Agric. For. Meteorol.* **2000**, *103*, 11–26. [CrossRef]
4. Pimentel, D.; Berger, B.; Filiberto, D.; Newton, M.; Wolfe, B.; Karabinakis, E.; Clark, S.; Poon, E.; Abbett, E.; Nandagopal, S. Water Resources: Agricultural and Environmental Issues. *BioScience* **2004**, *54*, 909–918. [CrossRef]
5. Gomiero, T.; Pimentel, D.; Paoletti, M.G. Environmental Impact of Different Agricultural Management Practices: Conventional vs. Organic Agriculture. *Crit. Rev. Plant Sci.* **2011**, *30*, 95–124. [CrossRef]
6. Zhang, N.; Wang, M.; Wang, N. Precision Agriculture—A Worldwide Overview. *Comput. Electron. Agric.* **2002**, *36*, 113–132. [CrossRef]
7. Gebbers, R.; Adamchuk, V.I. Precision Agriculture and Food Security. *Science* **2010**, *327*, 828–831. [CrossRef] [PubMed]
8. Maes, W.H.; Steppe, K. Perspectives for Remote Sensing with Unmanned Aerial Vehicles in Precision Agriculture. *Trends Plant Sci.* **2019**, *24*, 152–164. [CrossRef] [PubMed]
9. Weiss, M.; Jacob, F.; Duveiller, G. Remote Sensing for Agricultural Applications: A Meta-Review. *Remote Sens. Environ.* **2020**, *236*, 111402. [CrossRef]
10. Anastasiou, E.; Balafoutis, A.T.; Fountas, S. Trends in Remote Sensing Technologies in Olive Cultivation. *Smart Agric. Technol.* **2023**, *3*, 100103. [CrossRef]
11. Messina, G.; Modica, G. Twenty Years of Remote Sensing Applications Targeting Landscape Analysis and Environmental Issues in Olive Growing: A Review. *Remote Sens.* **2022**, *14*, 5430. [CrossRef]
12. Messina, G.; Modica, G. The Role of Remote Sensing in Olive Growing Farm Management: A Research Outlook from 2000 to the Present in the Framework of Precision Agriculture Applications. *Remote Sens.* **2022**, *14*, 5951. [CrossRef]
13. Roma, E.; Catania, P. Precision Oliviculture: Research Topics, Challenges, and Opportunities—A Review. *Remote Sens.* **2022**, *14*, 1668. [CrossRef]
14. Rodríguez-Garlito, E.C.; Paz-Gallardo, A. Efficiently Mapping Large Areas of Olive Trees Using Drones in Extremadura, Spain. *IEEE J. Miniaturiz. Air Space Syst.* **2021**, *2*, 148–156. [CrossRef]
15. Abubakar, M.A.; Chanzy, A.; Flamain, F.; Pouget, G.; Courault, D. Delineation of Orchard, Vineyard, and Olive Trees Based on Phenology Metrics Derived from Time Series of Sentinel-2. *Remote Sens.* **2023**, *15*, 2420. [CrossRef]
16. Osa, P.I.; Beck, A.-L.; Kleverman, L.; Mangin, A. Multi-Classifier Pipeline for Olive Groves Detection. *Appl. Sci.* **2023**, *13*, 420. [CrossRef]

17. Modica, G.; Messina, G.; De Luca, G.; Fiozzo, V.; Praticò, S. Monitoring the Vegetation Vigor in Heterogeneous Citrus and Olive Orchards. A Multiscale Object-Based Approach to Extract Trees' Crowns from UAV Multispectral Imagery. *Comput. Electron. Agric.* **2020**, *175*, 105500. [CrossRef]

18. Ruiz, L.A.; Almonacid-Caballer, J.; Crespo-Peremarch, P.; Recio, J.A.; Pardo-Pascual, J.E.; Sánchez-García, E. Automated Classification of Crop Types and Condition in a Mediterranean Area Using a Fine-Tuned Convolutional Neural Network. *Int. Arch. Photogramm. Remote Sens. Spat. Inf. Sci.* **2020**, *XLIII-B3-2020*, 1061–1068. [CrossRef]

19. Șandric, I.; Irimia, R.; Petropoulos, G.P.; Anand, A.; Srivastava, P.K.; Pleșoianu, A.; Faraslis, I.; Stateras, D.; Kalivas, D. Tree's Detection & Health's Assessment from Ultra-High Resolution UAV Imagery and Deep Learning. *Geocarto Int.* **2022**, *37*, 10459–10479.

20. Noguera, M.; Aquino, A.; Ponce, J.M.; Cordeiro, A.; Silvestre, J.; Arias-Calderón, R.; da Encarnação Marcelo, M.; Jordão, P.; Andújar, J.M. Nutritional Status Assessment of Olive Crops by Means of the Analysis and Modelling of Multispectral Images Taken with UAVs. *Biosyst. Eng.* **2021**, *211*, 1–18. [CrossRef]

21. Noguera, M.; Millán, B.; Pérez-Paredes, J.J.; Ponce, J.M.; Aquino, A.; Andújar, J.M. A New Low-Cost Device Based on Thermal Infrared Sensors for Olive Tree Canopy Temperature Measurement and Water Status Monitoring. *Remote Sens.* **2020**, *12*, 723. [CrossRef]

22. Marques, P.; Pádua, L.; Sousa, J.J.; Fernandes-Silva, A. Assessing the Water Status and Leaf Pigment Content of Olive Trees: Evaluating the Potential and Feasibility of Unmanned Aerial Vehicle Multispectral and Thermal Data for Estimation Purposes. *Remote Sens.* **2023**, *15*, 4777. [CrossRef]

23. Bchir, A.; M'nassri, S.; Dhib, S.; Amri, A.E.; Mulla, D. Estimating and Mapping Evapotranspiration in Olive Groves of Semi-Arid Tunisia Using Empirical Formulas and Satellite Remote Sensing. *Arab. J. Geosci.* **2021**, *14*, 2717. [CrossRef]

24. Elfarkh, J.; Johansen, K.; El Hajj, M.M.; Almashharawi, S.K.; McCabe, M.F. Evapotranspiration, Gross Primary Productivity and Water Use Efficiency over a High-Density Olive Orchard Using Ground and Satellite Based Data. *Agric. Water Manag.* **2023**, *287*, 108423. [CrossRef]

25. Spyropoulos, N.V.; Dalezios, N.R.; Kaltsis, I.; Faraslis, I.N. Very High Resolution Satellite-Based Monitoring of Crop (Olive Trees) Evapotranspiration in Precision Agriculture. *Int. J. Sustain. Agric. Manag. Inform.* **2020**, *6*, 22–42. [CrossRef]

26. Cuneo, P.; Jacobson, C.r.; Leishman, M.r. Landscape-Scale Detection and Mapping of Invasive African Olive (*Olea europaea* L. ssp. *Cuspidata* Wall Ex G. Don Ciferri) in SW Sydney, Australia Using Satellite Remote Sensing. *Appl. Veg. Sci.* **2009**, *12*, 145–154.

27. Alshammari, H.H.; Altaieb, M.O.; Boukrara, A.; Gasmi, K.; Aelmoniem, M. Expansion of the Olive Crop Based on Modeling Climatic Variables Using Geographic Information System (GIS) in Aljouf Region KSA. *Comput. Electron. Agric.* **2022**, *202*, 107280. [CrossRef]

28. Torres-Sánchez, J.; Mesas-Carrascosa, F.J.; Pérez-Porras, F.; López-Granados, F. Detection of Ecballium Elaterium in Hedgerow Olive Orchards Using a Low-Cost Uncrewed Aerial Vehicle and Open-Source Algorithms. *Pest Manag. Sci.* **2023**, *79*, 645–654. [CrossRef] [PubMed]

29. Castrignanò, A.; Belmonte, A.; Antelmi, I.; Quarto, R.; Quarto, F.; Shaddad, S.; Sion, V.; Muolo, M.R.; Ranieri, N.A.; Gadaleta, G.; et al. Semi-Automatic Method for Early Detection of *Xylella fastidiosa* in Olive Trees Using UAV Multispectral Imagery and Geostatistical-Discriminant Analysis. *Remote Sens.* **2021**, *13*, 14. [CrossRef]

30. Poblete, T.; Navas-Cortes, J.A.; Camino, C.; Calderon, R.; Hornero, A.; Gonzalez-Dugo, V.; Landa, B.B.; Zarco-Tejada, P.J. Discriminating *Xylella fastidiosa* from *Verticillium dahliae* Infections in Olive Trees Using Thermal- and Hyperspectral-Based Plant Traits. *ISPRS J. Photogramm. Remote Sens.* **2021**, *179*, 133–144. [CrossRef]

31. Mamalis, M.; Kalampokis, E.; Kalfas, I.; Tarabanis, K. Deep Learning for Detecting Verticillium Fungus in Olive Trees: Using YOLO in UAV Imagery. *Algorithms* **2023**, *16*, 343. [CrossRef]

32. Ortenzi, L.; Violino, S.; Pallottino, F.; Figorilli, S.; Vasta, S.; Tocci, F.; Antonucci, F.; Imperi, G.; Costa, C. Early Estimation of Olive Production from Light Drone Orthophoto, through Canopy Radius. *Drones* **2021**, *5*, 118. [CrossRef]

33. Sola-Guirado, R.R.; Castillo-Ruiz, F.J.; Jiménez-Jiménez, F.; Blanco-Roldan, G.L.; Castro-Garcia, S.; Gil-Ribes, J.A. Olive Actual "on Year" Yield Forecast Tool Based on the Tree Canopy Geometry Using UAS Imagery. *Sensors* **2017**, *17*, 1743. [CrossRef]

34. Khan, U.; Maqsood, M.; Gillani, S.; Durrani, M.Y.; Mehmood, I.; Seo, S. A Deep Learning-Based Framework for Accurate Identification and Crop Estimation of Olive Trees. *J. Supercomput.* **2023**, *79*, 1834–1855. [CrossRef]

35. Japón-Luján, R.; Luque-Rodríguez, J.M.; Luque de Castro, M.D. Dynamic Ultrasound-Assisted Extraction of Oleuropein and Related Biophenols from Olive Leaves. *J. Chromatogr. A* **2006**, *1108*, 76–82. [CrossRef] [PubMed]

36. Soni, M.G.; Burdock, G.A.; Christian, M.S.; Bitler, C.M.; Crea, R. Safety Assessment of Aqueous Olive Pulp Extract as an Antioxidant or Antimicrobial Agent in Foods. *Food Chem. Toxicol.* **2006**, *44*, 903–915. [CrossRef] [PubMed]

37. Fernandes-Silva, A.A.; Ferreira, T.C.; Correia, C.M.; Malheiro, A.C.; Villalobos, F.J. Influence of Different Irrigation Regimes on Crop Yield and Water Use Efficiency of Olive. *Plant Soil* **2010**, *333*, 35–47. [CrossRef]

38. Sanzani, S.M.; Schena, L.; Nigro, F.; Sergeeva, V.; Ippolito, A.; Salerno, M.G. Abiotic Diseases of Olive. *J. Plant Pathol.* **2012**, *94*, 469–491.

39. Zarco-Tejada, P.J.; Camino, C.; Beck, P.S.A.; Calderon, R.; Hornero, A.; Hernández-Clemente, R.; Kattenborn, T.; Montes-Borrego, M.; Susca, L.; Morelli, M.; et al. Previsual Symptoms of *Xylella fastidiosa* Infection Revealed in Spectral Plant-Trait Alterations. *Nat. Plants* **2018**, *4*, 432–439. [CrossRef]

40. Poblete, T.; Camino, C.; Beck, P.S.A.; Hornero, A.; Kattenborn, T.; Saponari, M.; Boscia, D.; Navas-Cortes, J.A.; Zarco-Tejada, P.J. Detection of *Xylella fastidiosa* Infection Symptoms with Airborne Multispectral and Thermal Imagery: Assessing Bandset Reduction Performance from Hyperspectral Analysis. *ISPRS J. Photogramm. Remote Sens.* **2020**, *162*, 27–40. [CrossRef]

41. Moher, D.; Liberati, A.; Tetzlaff, J.; Altman, D.G. Preferred Reporting Items for Systematic Reviews and Meta-Analyses: The PRISMA Statement. *Int. J. Surg.* **2010**, *8*, 336–341. [CrossRef]

42. Rouse, J.; Haas, R.; Schell, J.; Deering, D.; Harlan, J. *Monitoring the Vernal Advancements and Retrogradation*; NASA: Washington, DC, USA, 1974.

43. Pádua, L.; Vanko, J.; Hruška, J.; Adão, T.; Sousa, J.J.; Peres, E.; Morais, R. UAS, Sensors, and Data Processing in Agroforestry: A Review towards Practical Applications. *Int. J. Remote Sens.* **2017**, *38*, 2349–2391. [CrossRef]

44. Mulla, D.J. Twenty Five Years of Remote Sensing in Precision Agriculture: Key Advances and Remaining Knowledge Gaps. *Biosyst. Eng.* **2013**, *114*, 358–371. [CrossRef]

45. Bauer, M.; Cipra, J. *Identification of Agricultural Crops by Computer Processing of ERTS MSS Data*; LARS Technical Report; Laboratory for Applications of Remote Sensing: Lafayette, IN, USA, 1973.

46. Alganci, U.; Sertel, E.; Kaya, S. Determination of the Olive Trees with Object Based Classification of Pleiades Satellite Image. *Int. J. Environ. Geoinformat.* **2018**, *5*, 132–139. [CrossRef]

47. Akcay, H.; Kaya, S.; Sertel, E.; Alganci, U. Determination of Olive Trees with Multi-Sensor Data Fusion. In Proceedings of the 2019 8th International Conference on Agro-Geoinformatics (Agro-Geoinformatics), Istanbul, Turkey, 16–19 July 2019; pp. 1–6.

48. Huang, Y.; Thomson, S.J.; Brand, H.J.; Reddy, K.N. Development and Evaluation of Low-Altitude Remote Sensing Systems for Crop Production Management. *Int. J. Agric. Biol. Eng.* **2016**, *9*, 1–11.

49. Candiago, S.; Remondino, F.; De Giglio, M.; Dubbini, M.; Gattelli, M. Evaluating Multispectral Images and Vegetation Indices for Precision Farming Applications from UAV Images. *Remote Sens.* **2015**, *7*, 4026–4047. [CrossRef]

50. Paço, T.A.; Pôças, I.; Cunha, M.; Silvestre, J.C.; Santos, F.L.; Paredes, P.; Pereira, L.S. Evapotranspiration and Crop Coefficients for a Super Intensive Olive Orchard. An Application of SIMDualKc and METRIC Models Using Ground and Satellite Observations. *J. Hydrol.* **2014**, *519*, 2067–2080. [CrossRef]

51. Pôças, I.; Paço, T.A.; Cunha, M.; Andrade, J.A.; Silvestre, J.; Sousa, A.; Santos, F.L.; Pereira, L.S.; Allen, R.G. Satellite-Based Evapotranspiration of a Super-Intensive Olive Orchard: Application of METRIC Algorithms. *Biosyst. Eng.* **2014**, *128*, 69–81. [CrossRef]

52. Sparks, A.M.; Bouhamed, I.; Boschetti, L.; Gitas, I.Z.; Kalaitzidis, C. Mapping Arable Land and Permanent Agriculture Extent and Change in Southern Greece Using the European Union LUCAS Survey and a 35-Year Landsat Time Series Analysis. *Remote Sens.* **2022**, *14*, 3369. [CrossRef]

53. Kharrou, M.H.; Simonneaux, V.; Er-Raki, S.; Le Page, M.; Khabba, S.; Chehbouni, A. Assessing Irrigation Water Use with Remote Sensing-Based Soil Water Balance at an Irrigation Scheme Level in a Semi-Arid Region of Morocco. *Remote Sens.* **2021**, *13*, 1133. [CrossRef]

54. Pieri, M.; Cantini, C.; Giovannelli, A.; Maselli, F.; Chiesi, M.; Battista, P.; Fibbi, L.; Gardin, L.; Rapi, B.; Romani, M.; et al. Estimation of Actual Evapotranspiration in Fragmented Mediterranean Areas by the Spatio-Temporal Fusion of NDVI Data. *IEEE J. Sel. Top. Appl. Earth Obs. Remote Sens.* **2019**, *12*, 5108–5117. [CrossRef]

55. Häusler, M.; Conceição, N.; Tezza, L.; Sánchez, J.M.; Campagnolo, M.L.; Häusler, A.J.; Silva, J.M.N.; Warneke, T.; Heygster, G.; Ferreira, M.I. Estimation and Partitioning of Actual Daily Evapotranspiration at an Intensive Olive Grove Using the STSEB Model Based on Remote Sensing. *Agric. Water Manag.* **2018**, *201*, 188–198. [CrossRef]

56. Pôças, I.; Paço, T.A.; Paredes, P.; Cunha, M.; Pereira, L.S. Estimation of Actual Crop Coefficients Using Remotely Sensed Vegetation Indices and Soil Water Balance Modelled Data. *Remote Sens.* **2015**, *7*, 2373–2400. [CrossRef]

57. Unal, E.; Mermer, A.; Dogan, H.M. Determining Major Orchard (Pistachio, Olive, Vineyard) Areas in Gaziantep Province Using Remote Sensing Techniques. *Int. Arch. Photogramm. Remote Sens. Spat. Inf. Sci.* **2004**, *35 (Part B7)*, 160–163.

58. Torkashvand, A.M.; Shadparvar, V. Proposing a Methodology in Preparation of Olive Orchards Map by Remote Sensing and Geographic Information System. In Proceedings of the 19th International Conference on GeoInformatics, Shanghai, China, 24–26 June 2011; pp. 1–6.

59. Torkashvand, A.M.; Zahedi, S.S. Providing a Supervised Map of Olive Orchards by IRS Satellite Images. *Life Sci. J.* **2011**, *8*, 127–133.

60. Maselli, F.; Chiesi, M.; Brilli, L.; Moriondo, M. Simulation of Olive Fruit Yield in Tuscany through the Integration of Remote Sensing and Ground Data. *Ecol. Model.* **2012**, *244*, 1–12. [CrossRef]

61. Ortega-Farías, S.; Ortega-Salazar, S.; Aguilar, R.; de la Fuente, D.; Fuentes, F. Evaluation of a Model to Estimate Net Radiation over a Drip-Irrigated Olive Orchard Using Landsat Satellite Images. *Acta Hortic.* **2014**, 309–314. [CrossRef]

62. Fuentes-Peñailillo, F.; Ortega-Farías, S.; Acevedo-Opazo, C.; Fonseca-Luengo, D. Implementation of a Two-Source Model for Estimating the Spatial Variability of Olive Evapotranspiration Using Satellite Images and Ground-Based Climate Data. *Water* **2018**, *10*, 339. [CrossRef]

63. Yildirim, T.; Zhou, Y.; Flynn, K.C.; Gowda, P.H.; Ma, S.; Moriasi, D.N. Evaluating the Sensitivity of Vegetation and Water Indices to Monitor Drought for Three Mediterranean Crops. *Agron. J.* **2021**, *113*, 123–134. [CrossRef]

64. Elfarkh, J.; Er-Raki, S.; Ezzahar, J.; Chehbouni, A.; Aithssaine, B.; Amazirh, A.; Khabba, S.; Jarlan, L. Integrating Thermal Stress Indexes within Shuttleworth–Wallace Model for Evapotranspiration Mapping over a Complex Surface. *Irrig. Sci.* **2021**, *39*, 45–61. [CrossRef]

65. Ortega-Salazar, S.; Ortega-Farías, S.; Kilic, A.; Allen, R. Performance of the METRIC Model for Mapping Energy Balance Components and Actual Evapotranspiration over a Superintensive Drip-Irrigated Olive Orchard. *Agric. Water Manag.* **2021**, *251*, 106861. [CrossRef]

66. Castelli, G.; Oliveira, L.A.A.; Abdelli, F.; Dhaou, H.; Bresci, E.; Ouessar, M. Effect of Traditional Check Dams (Jessour) on Soil and Olive Trees Water Status in Tunisia. *Sci. Total Environ.* **2019**, *690*, 226–236. [CrossRef]

67. Ramírez-Cuesta, J.M.; Kilic, A.; Allen, R.; Santos, C.; Lorite, I.J. Evaluating the Impact of Adjusting Surface Temperature Derived from Landsat 7 ETM+ in Crop Evapotranspiration Assessment Using High-Resolution Airborne Data. *Int. J. Remote Sens.* **2017**, *38*, 4177–4205. [CrossRef]

68. Bazi, Y.; Al-Sharari, H.; Melgani, F. An Automatic Method for Counting Olive Trees in Very High Spatial Remote Sensing Images. In Proceedings of the 2009 IEEE International Geoscience and Remote Sensing Symposium, Cape Town, South Africa, 12–17 July 2009; Volume 2, pp. 125–128.

69. Alexakis, D.D.; Sarris, A.; Kalaitzidis, C.; Papadopoulos, N.; Soupios, P. Integrated Use of Satellite Remote Sensing, GIS, and Ground Spectroscopy Techniques for Monitoring Olive Oil Mill Waste Disposal Areas on the Island of Crete, Greece. *Int. J. Remote Sens.* **2016**, *37*, 669–693. [CrossRef]

70. Masson, J.; Soille, P.; Mueller, R. Tests with VHR Images for the Identification of Olive Trees and Other Fruit Trees in the European Union. In Proceedings of the Remote Sensing for Agriculture, Ecosystems, and Hydrology VI, Maspalomas, Spain, 26 October 2004; SPIE: Bellingham, DC, USA, 2004; Volume 5568, pp. 23–36.

71. Karantzalos, K.; Argialas, D. Improving Edge Detection and Watershed Segmentation with Anisotropic Diffusion and Morphological Levellings. *Int. J. Remote Sens.* **2006**, *27*, 5427–5434. [CrossRef]

72. Semeraro, T.; Buccolieri, R.; Vergine, M.; De Bellis, L.; Luvisi, A.; Emmanuel, R.; Marwan, N. Analysis of Olive Grove Destruction by *Xylella fastidiosa* Bacterium on the Land Surface Temperature in Salento Detected Using Satellite Images. *Forests* **2021**, *12*, 1266. [CrossRef]

73. Battista, P.; Chiesi, M.; Rapi, B.; Romani, M.; Cantini, C.; Giovannelli, A.; Cocozza, C.; Tognetti, R.; Maselli, F. Integration of Ground and Multi-Resolution Satellite Data for Predicting the Water Balance of a Mediterranean Two-Layer Agro-Ecosystem. *Remote Sens.* **2016**, *8*, 731. [CrossRef]

74. Blum, M.; Lensky, I.M.; Nestel, D. Estimation of Olive Grove Canopy Temperature from MODIS Thermal Imagery Is More Accurate than Interpolation from Meteorological Stations. *Agric. For. Meteorol.* **2013**, *176*, 90–93. [CrossRef]

75. Telesca, L.; Abate, N.; Faridani, F.; Lovallo, M.; Lasaponara, R. Discerning Xylella Fastidiosa-Infected Olive Orchards in the Time Series of MODIS Terra Satellite Evapotranspiration Data by Using the Fisher–Shannon Analysis and the Multifractal Detrended Fluctuation Analysis. *Fractal Fract.* **2023**, *7*, 466. [CrossRef]

76. Telesca, L.; Abate, N.; Faridani, F.; Lovallo, M.; Lasaponara, R. Revealing Traits of Phytopathogenic Status Induced by *Xylella fastidiosa* in Olive Trees by Analysing Multifractal and Informational Patterns of MODIS Satellite Evapotranspiration Data. *Phys. Stat. Mech. Its Appl.* **2023**, *629*, 129163. [CrossRef]

77. Brilli, L.; Chiesi, M.; Maselli, F.; Moriondo, M.; Gioli, B.; Toscano, P.; Zaldei, A.; Bindi, M. Simulation of Olive Grove Gross Primary Production by the Combination of Ground and Multi-Sensor Satellite Data. *Int. J. Appl. Earth Obs. Geoinf.* **2013**, *23*, 29–36. [CrossRef]

78. Sepulcre-Canto, G.; Zarco-Tejada, P.J.; Jimenez-Berni, J.A.; Rodriguez, A.J.; Jimenez-Munoz, J.C.; Sobrino, J.A.; Cifuentes, V. Detecting Crop Irrigation Status in Orchard Canopies with Airborne and ASTER Thermal Imagery. In Proceedings of the 2007 IEEE International Geoscience and Remote Sensing Symposium, Barcelona, Spain, 23–28 July 2007; pp. 3643–3646.

79. González, J.; Galindo, C.; Arevalo, V.; Ambrosio, G. Applying Image Analysis and Probabilistic Techniques for Counting Olive Trees in High-Resolution Satellite Images. In Proceedings of the Advanced Concepts for Intelligent Vision Systems; Blanc-Talon, J., Philips, W., Popescu, D., Scheunders, P., Eds.; Springer: Berlin/Heidelberg, Germany, 2007; pp. 920–931.

80. García Torres, L.; Peña-Barragán, J.M.; López-Granados, F.; Jurado-Expósito, M.; Fernández-Escobar, R. Automatic Assessment of Agro-Environmental Indicators from Remotely Sensed Images of Tree Orchards and Its Evaluation Using Olive Plantations. *Comput. Electron. Agric.* **2008**, *61*, 179–191. [CrossRef]

81. Gómez, J.A.; Zarco-Tejada, P.J.; García-Morillo, J.; Gama, J.; Soriano, M.A. Determining Biophysical Parameters for Olive Trees Using CASI-Airborne and Quickbird-Satellite Imagery. *Agron. J.* **2011**, *103*, 644–654. [CrossRef]

82. Castillejo-González, I. Mapping of Olive Trees Using Pansharpened QuickBird Images: An Evaluation of Pixel- and Object-Based Analyses. *Agronomy* **2018**, *8*, 288. [CrossRef]

83. Apan, A.; Young, F.R.; Phinn, S.; Held, A.; Favier, J. Mapping Olive Varieties and within-Field Spatial Variability Using High Resolution QuickBird Imagery. In Proceedings of the 12th Australasian Remote Sensing and Photogrammetry Conference, Fremantle, Australia, 18–22 October 2004; Spatial Sciences Institute: Los Angeles, CA, USA, 2004.

84. Karydas, C.G.; Sekuloska, T.; Silleos, G.N. Quantification and Site-Specification of the Support Practice Factor When Mapping Soil Erosion Risk Associated with Olive Plantations in the Mediterranean Island of Crete. *Environ. Monit. Assess.* **2009**, *149*, 19–28. [CrossRef] [PubMed]

85. Peña-Barragán, J.M.; López-Granados, F.; García-Torres, L.; Jurado-Expósito, M.; Sánchez de la Orden, M.; García-Ferrer, A. Discriminating Cropping Systems and Agro-Environmental Measures by Remote Sensing. *Agron. Sustain. Dev.* **2008**, *28*, 355–362. [CrossRef]

86. Navarro, R.; Wirkus, L.; Dubovyk, O. Spatio-Temporal Assessment of Olive Orchard Intensification in the Saïss Plain (Morocco) Using k-Means and High-Resolution Satellite Data. *Remote Sens.* **2023**, *15*, 50. [CrossRef]

87. Kurucu, Y.; Esetlili, T.; Erden, H.; Öztürk, G.; Güven, A.İ.; Çamaşırcıoğlu, E. Digitalization of Olive Trees by Using Remote Sensing Techniques. In Proceedings of the 2015 Fourth International Conference on Agro-Geoinformatics (Agro-geoinformatics), Istanbul, Turkey, 20–24 July 2015; pp. 121–124.

88. Lin, C.; Jin, Z.; Mulla, D.; Ghosh, R.; Guan, K.; Kumar, V.; Cai, Y. Toward Large-Scale Mapping of Tree Crops with High-Resolution Satellite Imagery and Deep Learning Algorithms: A Case Study of Olive Orchards in Morocco. *Remote Sens.* **2021**, *13*, 1740. [CrossRef]

89. Poblete, T.; Navas-Cortes, J.A.; Hornero, A.; Camino, C.; Calderon, R.; Hernandez-Clemente, R.; Landa, B.B.; Zarco-Tejada, P.J. Detection of Symptoms Induced by Vascular Plant Pathogens in Tree Crops Using High-Resolution Satellite Data: Modelling and Assessment with Airborne Hyperspectral Imagery. *Remote Sens. Environ.* **2023**, *295*, 113698. [CrossRef]

90. Belfiore, O.R.; Aguilar, M.A.; Parente, C. Processing Very High-Resolution Satellite Images for Individual Tree Identification with Local Maxima Method. In *Proceedings of the R3 in Geomatics: Research, Results and Review*; Parente, C., Troisi, S., Vettore, A., Eds.; Springer International Publishing: Cham, Switzerland, 2020; pp. 323–335.

91. Blonda, P.; Tarantino, C.; Scortichini, M.; Maggi, S.; Tarantino, M.; Adamo, M. Satellite Monitoring of Bio-Fertilizer Restoration in Olive Groves Affected by *Xylella fastidiosa* Subsp. *Pauca*. *Sci. Rep.* **2023**, *13*, 5695. [CrossRef] [PubMed]

92. Kefi, M.; Pham, T.D.; Kashiwagi, K.; Yoshino, K. Identification of Irrigated Olive Growing Farms Using Remote Sensing Techniques. *Euro-Mediterr. J. Environ. Integr.* **2016**, *1*, 3. [CrossRef]

93. Reyes Rojas, L.A.; Moletto-Lobos, I.; Corradini, F.; Mattar, C.; Fuster, R.; Escobar-Avaria, C. Determining Actual Evapotranspiration Based on Machine Learning and Sinusoidal Approaches Applied to Thermal High-Resolution Remote Sensing Imagery in a Semi-Arid Ecosystem. *Remote Sens.* **2021**, *13*, 4105. [CrossRef]

94. Kefi, M.; Pham, T.D.; Ha, N.T.; Kenichi, K. Assessment of Drought Impact on Agricultural Production Using Remote Sensing and Machine Learning Techniques in Kairouan Prefecture, Tunisia. In *Applications of Space Techniques on the Natural Hazards in the MENA Region*; Al Saud, M.M., Ed.; Springer International Publishing: Cham, Switzerland, 2022; pp. 401–418, ISBN 978-3-030-88874-9.

95. Mezzi, R.; Alioscha-Perez, M.; Allani, M.; Guedri, F.; Zouabi, A.; Beji, R.; Sahli, H.; Sahli, A. Olive Tree Classification and Inventory with Medium Resolution Multi-Spectral Satellite Imagery. In *Space Fostering African Societies: Developing the African Continent through Space, Part 1*; Springer: Berlin/Heidelberg, Germany, 2020; pp. 13–30.

96. Solano, F.; Di Fazio, S.; Modica, G. A Methodology Based on GEOBIA and WorldView-3 Imagery to Derive Vegetation Indices at Tree Crown Detail in Olive Orchards. *Int. J. Appl. Earth Obs. Geoinf.* **2019**, *83*, 101912. [CrossRef]

97. Domazetovic, F.; Siljeg, A.; Maric, I.; Jurisic, M. Assessing the Vertical Accuracy of Worldview-3 Stereo-Extracted Digital Surface Model over Olive Groves. *GISTAM* **2020**, *246*, 253.

98. Rivera, A.J.; Pérez-Godoy, M.D.; Elizondo, D.; Deka, L.; del Jesus, M.J. A Preliminary Study on Crop Classification with Unsupervised Algorithms for Time Series on Images with Olive Trees and Cereal Crops. In Proceedings of the 15th International Conference on Soft Computing Models in Industrial and Environmental Applications (SOCO 2020), Burgos, Spain, 16–18 September 2020; Springer International Publishing: Cham, Switzerland, 2021; pp. 276–285.

99. Hornero, A.; Hernández-Clemente, R.; North, P.R.J.; Beck, P.S.A.; Boscia, D.; Navas-Cortes, J.A.; Zarco-Tejada, P.J. Monitoring the Incidence of *Xylella fastidiosa* Infection in Olive Orchards Using Ground-Based Evaluations, Airborne Imaging Spectroscopy and Sentinel-2 Time Series through 3-D Radiative Transfer Modelling. *Remote Sens. Environ.* **2020**, *236*, 111480. [CrossRef]

100. Makhloufi, A.; Kallel, A.; Chaker, R.; Gastellu-Etchegorry, J.-P. Retrieval of Olive Tree Biophysical Properties from Sentinel-2 Time Series Based on Physical Modelling and Machine Learning Technique. *Int. J. Remote Sens.* **2021**, *42*, 8542–8571. [CrossRef]

101. Moral, F.J.; Rebollo, F.J.; Millán, S.; Prieto, H.; Pérez, J.M.; Campillo, C. Can Satellite-Derived Vigour Maps Be Used to Delineate Homogeneous Zones in Hedgerow Olive Orchards? In *Precision Agriculture'19*; Wageningen Academic Publishers: Wageningen, The Netherlands, 2019; pp. 477–483. ISBN 978-90-8686-337-2.

102. Abdelmoula, H.; Kallel, A.; Roujean, J.-L.; Gastellu-Etchegorry, J.-P. Dynamic Retrieval of Olive Tree Properties Using Bayesian Model and Sentinel-2 Images. *IEEE J. Sel. Top. Appl. Earth Obs. Remote Sens.* **2021**, *14*, 9267–9286. [CrossRef]

103. Blázquez-Carrasco, Á.; Gómez-Giráldez, P.J.; Castro-Rodríguez, J.; Colombo, S.; Carpintero, E.; González-Dugo, M.P. Estimation of Olive Groves Cover Crops Net Primary Productivity Using Remote Sensing Data. In *Remote Sensing for Agriculture, Ecosystems, and Hydrology XXIII*; SPIE: Bellingham, WA, USA, 2021; Volume 11856, p. 118560S.

104. Navrozidis, I.; Alexandridis, T.; Moshou, D.; Haugommard, A.; Lagopodi, A. Implementing Sentinel-2 Data and Machine Learning to Detect Plant Stress in Olive Groves. *Remote Sens.* **2022**, *14*, 5947. [CrossRef]

105. Leolini, L.; Moriondo, M.; Rossi, R.; Bellini, E.; Brilli, L.; López-Bernal, Á.; Santos, J.A.; Fraga, H.; Bindi, M.; Dibari, C.; et al. Use of Sentinel-2 Derived Vegetation Indices for Estimating fPAR in Olive Groves. *Agronomy* **2022**, *12*, 1540. [CrossRef]

106. Chiesi, M.; Costafreda-Aumedes, S.; Argenti, G.; Battista, P.; Fibbi, L.; Leolini, L.; Moriondo, M.; Rapi, B.; Sabatini, F.; Maselli, F. Estimating the GPP of Olive Trees with Variable Canopy Cover by the Use of Sentinel-2 MSI Images. *Eur. J. Agron.* **2022**, *141*, 126618. [CrossRef]

107. Panagiotopoulou, A.; Charou, E.; Poirazidis, K.; Voutos, Y.; Martinis, A.; Grammatikopoulos, L.; Petsa, E.; Bratsolis, E.; Mylonas, P. Deep-Learning Based Super-Resolution of Sentinel-2 Images for Monitoring Supercentenarian Olive Trees. In Proceedings of the 25th Pan-Hellenic Conference on Informatics, Volos, Greece, 26–28 November 2021; Association for Computing Machinery: New York, NY, USA, 2022; pp. 143–148.

108. Guermazi, E.; Wali, A.; Ksibi, M. Combining Remote Sensing, SPAD Readings, and Laboratory Analysis for Monitoring Olive Groves and Olive Oil Quality. *Precis. Agric.* **2023**, *25*, 65–82. [CrossRef]

109. Volpi, I.; Marchi, S.; Petacchi, R.; Hoxha, K.; Guidotti, D. Detecting Olive Grove Abandonment with Sentinel-2 and Machine Learning: The Development of a Web-Based Tool for Land Management. *Smart Agric. Technol.* **2023**, *3*, 100068. [CrossRef]

110. Battista, P.; Bellini, E.; Chiesi, M.; Costafreda-Aumedes, S.; Fibbi, L.; Leolini, L.; Moriondo, M.; Rapi, B.; Rossi, R.; Sabatini, F.; et al. Estimating the Effect of Water Shortage on Olive Trees by the Combination of Meteorological and Sentinel-2 Data. *Eur. J. Remote Sens.* **2023**, *56*, 2194553. [CrossRef]

111. Shaik, R.U.; Jallu, S.B.; Doctor, K. Unveiling Temperature Patterns in Tree Canopies across Diverse Heights and Types. *Remote Sens.* **2023**, *15*, 2080. [CrossRef]

112. Chiraz, M.C.; Olfa, M.; Hamadi, H. Remote Sensing and Soil Moisture Data for Water Productivity Determination. *Agric. Water Manag.* **2022**, *263*, 107482. [CrossRef]

113. Martínez-Ruedas, C.; Guerrero-Ginel, J.E.; Fernández-Ahumada, E. Methodology for the Automatic Inventory of Olive Groves at the Plot and Polygon Level. *Agronomy* **2022**, *12*, 1735. [CrossRef]

114. Dindaroğlu, T.; Kılıç, M.; Günal, E.; Gündoğan, R.; Akay, A.E.; Seleiman, M. Multispectral UAV and Satellite Images for Digital Soil Modeling with Gradient Descent Boosting and Artificial Neural Network. *Earth Sci. Inform.* **2022**, *15*, 2239–2263. [CrossRef]

115. Cantini, C.; Nepi, P.E.; Avola, G.; Riggi, E. Direct and Indirect Ground Estimation of Leaf Area Index to Support Interpretation of NDVI Data from Satellite Images in Hedgerow Olive Orchards. *Smart Agric. Technol.* **2023**, *5*, 100267. [CrossRef]

116. Hachicha, M.; Kallel, A.; Louati, M. Prediction of Plant Growth Based on Statistical Methods and Remote Sensing Data. *J. Appl. Remote Sens.* **2021**, *15*, 042410. [CrossRef]

117. Panagiotopoulou, A.; Bratsolis, E.; Grammatikopoulos, L.; Petsa, E.; Charou, E.; Poirazidis, K.; Martinis, A.; Madamopoulos, N. Sentinel-2 Images at 2.5 m Spatial Resolution via Deep-Learning: A Case Study in Zakythnos. In Proceedings of the 2022 IEEE 14th Image, Video, and Multidimensional Signal Processing Workshop (IVMSP), Nafplio, Greece, 26–29 June 2022.

118. Aguirre-García, S.-D.; Aranda-Barranco, S.; Nieto, H.; Serrano-Ortiz, P.; Sánchez-Cañete, E.-P.; Guerrero-Rascado, J.-L. Modelling Actual Evapotranspiration Using a Two Source Energy Balance Model with Sentinel Imagery in Herbaceous-Free and Herbaceous-Cover Mediterranean Olive Orchards. *Agric. For. Meteorol.* **2021**, *311*, 108692. [CrossRef]

119. Ioannis, N.; Alexandridis, T.K.; Moshou, D.; Pantazi, X.E.; Alexandra Tamouridou, A.; Kozhukh, D.; Castef, F.; Lagopodi, A.; Zartaloudis, Z.; Mourelatos, S.; et al. Olive Trees Stress Detection Using Sentinel-2 Images. In Proceedings of the IGARSS 2019—2019 IEEE International Geoscience and Remote Sensing Symposium, Yokohama, Japan, 28 July–2 August 2019; pp. 7220–7223.

120. Abdelmoula, H.; Kallel, A.; Rouiean, L.-L.; Chaabouni, S.; Gargouri, K.; Ghrab, M.; Gastellu-Etchegorry, J.-P.; Lauret, N. *Olive Biophysical Property Estimation Based on Sentinel-2 Image Inversion*; IEEE: Piscataway, NJ, USA, 2018; pp. 2869–2872.

121. Abdelmoula, H.; Kallel, A.; Roujean, J.-L.; Chaabouni, S.; Gargouri, K.; Ghrab, M.; Gastellu-Etchegorry, J.-P.; Lauret, N. Bayesian Inversion Technique of Olive Tree Biophysical Properties Using Sentinel-2 Images. In Proceedings of the 2018 4th International Conference on Advanced Technologies for Signal and Image Processing (ATSIP), Sousse, Tunisia, 21–24 March 2018; pp. 1–5.

122. Hornero, A.; Hernández-Clemente, R.; Beck, P.S.A.; Navas-Cortés, J.A.; Zarco-Tejada, P.J. Using Sentinel-2 Imagery to Track Changes Produced by *Xylella fastidiosa* in Olive Trees. In Proceedings of the IGARSS 2018—2018 IEEE International Geoscience and Remote Sensing Symposium, Valencia, Spain, 22–27 July 2018; pp. 9060–9062.

123. Brinkhoff, J.; Schultz, A.; Suarez, L.A.; Robson, A.J. Olive Tree Water Stress Detection Using Daily Multispectral Imagery. In Proceedings of the 2021 IEEE International Geoscience and Remote Sensing Symposium IGARSS, Brussels, Belgium, 11–16 July 2021; pp. 5826–5829.

124. Matese, A.; Toscano, P.; Di Gennaro, S.F.; Genesio, L.; Vaccari, F.P.; Primicerio, J.; Belli, C.; Zaldei, A.; Bianconi, R.; Gioli, B. Intercomparison of UAV, Aircraft and Satellite Remote Sensing Platforms for Precision Viticulture. *Remote Sens.* **2015**, *7*, 2971–2990. [CrossRef]

125. Berni, J.A.J.; Zarco-Tejada, P.J.; Sepulcre-Cantó, G.; Fereres, E.; Villalobos, F. Mapping Canopy Conductance and CWSI in Olive Orchards Using High Resolution Thermal Remote Sensing Imagery. *Remote Sens. Environ.* **2009**, *113*, 2380–2388. [CrossRef]

126. Calderón, R.; Navas-Cortés, J.A.; Zarco-Tejada, P.J. Early Detection and Quantification of *Verticillium* Wilt in Olive Using Hyperspectral and Thermal Imagery over Large Areas. *Remote Sens.* **2015**, *7*, 5584–5610. [CrossRef]

127. Estornell, J.; Velázquez-Martí, B.; López-Cortés, I.; Salazar, D.; Fernández-Sarría, A. Estimation of Wood Volume and Height of Olive Tree Plantations Using Airborne Discrete-Return LiDAR Data. *GIScience Remote Sens.* **2014**, *51*, 17–29. [CrossRef]

128. Alvarez-Vanhard, E.; Corpetti, T.; Houet, T. UAV & Satellite Synergies for Optical Remote Sensing Applications: A Literature Review. *Sci. Remote Sens.* **2021**, *3*, 100019.

129. Herwitz, S.R.; Johnson, L.F.; Dunagan, S.E.; Higgins, R.G.; Sullivan, D.V.; Zheng, J.; Lobitz, B.M.; Leung, J.G.; Gallmeyer, B.A.; Aoyagi, M.; et al. Imaging from an Unmanned Aerial Vehicle: Agricultural Surveillance and Decision Support. *Comput. Electron. Agric.* **2004**, *44*, 49–61. [CrossRef]

130. Berni, J.A.J.; Zarco-Tejada, P.J.; Suarez, L.; Fereres, E. Thermal and Narrowband Multispectral Remote Sensing for Vegetation Monitoring from an Unmanned Aerial Vehicle. *IEEE Trans. Geosci. Remote Sens.* **2009**, *47*, 722–738. [CrossRef]

131. Zarco-Tejada, P.J.; Guillén-Climent, M.L.; Hernández-Clemente, R.; Catalina, A.; González, M.R.; Martín, P. Estimating Leaf Carotenoid Content in Vineyards Using High Resolution Hyperspectral Imagery Acquired from an Unmanned Aerial Vehicle (UAV). *Agric. For. Meteorol.* **2013**, *171–172*, 281–294. [CrossRef]

132. Quiróz, R. Remote Sensing as a Monitoring Tool for Cropping Area Determination in Smallholder Agriculture in Tanzania and Uganda. 2015. Available online: https://hdl.handle.net/10568/69110 (accessed on 8 January 2024).

133. Pajares, G. Overview and Current Status of Remote Sensing Applications Based on Unmanned Aerial Vehicles (UAVs). *Photogramm. Eng. Remote Sens.* **2015**, *81*, 281–330. [CrossRef]

134. Torres-Sánchez, J.; López-Granados, F.; Borra-Serrano, I.; Peña, J.M. Assessing UAV-Collected Image Overlap Influence on Computation Time and Digital Surface Model Accuracy in Olive Orchards. *Precis. Agric.* **2018**, *19*, 115–133. [CrossRef]

135. Torres-Sánchez, J.; López-Granados, F.; Serrano, N.; Arquero, O.; Peña, J.M. High-Throughput 3-D Monitoring of Agricultural-Tree Plantations with Unmanned Aerial Vehicle (UAV) Technology. *PLoS ONE* **2015**, *10*, e0130479. [CrossRef]

136. de Castro, A.I.; Rallo, P.; Suárez, M.P.; Torres-Sánchez, J.; Casanova, L.; Jiménez-Brenes, F.M.; Morales-Sillero, A.; Jiménez, M.R.; López-Granados, F. High-Throughput System for the Early Quantification of Major Architectural Traits in Olive Breeding Trials Using UAV Images and OBIA Techniques. *Front. Plant Sci.* **2019**, *10*, 1472. [CrossRef]

137. Jiménez-Brenes, F.M.; López-Granados, F.; de Castro, A.I.; Torres-Sánchez, J.; Serrano, N.; Peña, J.M. Quantifying Pruning Impacts on Olive Tree Architecture and Annual Canopy Growth by Using UAV-Based 3D Modelling. *Plant Methods* **2017**, *13*, 55. [CrossRef] [PubMed]

138. Rallo, P.; de Castro, A.I.; López-Granados, F.; Morales-Sillero, A.; Torres-Sánchez, J.; Jiménez, M.R.; Jiménez-Brenes, F.M.; Casanova, L.; Suárez, M.P. Exploring UAV-Imagery to Support Genotype Selection in Olive Breeding Programs. *Sci. Hortic.* **2020**, *273*, 109615. [CrossRef]

139. Torres-Sánchez, J.; de la Rosa, R.; León, L.; Jiménez-Brenes, F.M.; Kharrat, A.; López-Granados, F. Quantification of Dwarfing Effect of Different Rootstocks in 'Picual' Olive Cultivar Using UAV-Photogrammetry. *Precis. Agric.* **2022**, *23*, 178–193. [CrossRef]

140. Egea, G.; Padilla-Díaz, C.M.; Martinez-Guanter, J.; Fernández, J.E.; Pérez-Ruiz, M. Assessing a Crop Water Stress Index Derived from Aerial Thermal Imaging and Infrared Thermometry in Super-High Density Olive Orchards. *Agric. Water Manag.* **2017**, *187*, 210–221. [CrossRef]

141. Martinez-Guanter, J.; Agüera, P.; Agüera, J.; Pérez-Ruiz, M. Spray and Economics Assessment of a UAV-Based Ultra-Low-Volume Application in Olive and Citrus Orchards. *Precis. Agric.* **2020**, *21*, 226–243. [CrossRef]

142. Caruso, G.; Palai, G.; Marra, F.P.; Caruso, T. High-Resolution UAV Imagery for Field Olive (*Olea europaea* L.) Phenotyping. *Horticulturae* **2021**, *7*, 258. [CrossRef]

143. Caruso, G.; Palai, G.; Gucci, R.; Priori, S. Remote and Proximal Sensing Techniques for Site-Specific Irrigation Management in the Olive Orchard. *Appl. Sci.* **2022**, *12*, 1309. [CrossRef]

144. Caruso, G.; Palai, G.; Tozzini, L.; Gucci, R. Using Visible and Thermal Images by an Unmanned Aerial Vehicle to Monitor the Plant Water Status, Canopy Growth and Yield of Olive Trees (Cvs. Frantoio and Leccino) under Different Irrigation Regimes. *Agronomy* **2022**, *12*, 1904. [CrossRef]

145. Caruso, G.; Zarco-Tejada, P.J.; González-Dugo, V.; Moriondo, M.; Tozzini, L.; Palai, G.; Rallo, G.; Hornero, A.; Primicerio, J.; Gucci, R. High-Resolution Imagery Acquired from an Unmanned Platform to Estimate Biophysical and Geometrical Parameters of Olive Trees under Different Irrigation Regimes. *PLoS ONE* **2019**, *14*, e0210804. [CrossRef]

146. Fernández, T.; Pérez, J.L.; Cardenal, J.; Gómez, J.M.; Colomo, C.; Delgado, J. Analysis of Landslide Evolution Affecting Olive Groves Using UAV and Photogrammetric Techniques. *Remote Sens.* **2016**, *8*, 837. [CrossRef]

147. Stateras, D.; Kalivas, D. Assessment of Olive Tree Canopy Characteristics and Yield Forecast Model Using High Resolution UAV Imagery. *Agriculture* **2020**, *10*, 385. [CrossRef]

148. Sarabia, R.; Aquino, A.; Ponce, J.M.; López, G.; Andújar, J.M. Automated Identification of Crop Tree Crowns from UAV Multispectral Imagery by Means of Morphological Image Analysis. *Remote Sens.* **2020**, *12*, 748. [CrossRef]

149. Çoşlu, M.; Sönmez, N.K. Determination of Olive Tree (*Olea europaea* L.) Some Dendrometric Components from Unmanned Aerial Vehicle (UAV) Data with Local Extrema and Multiresolution Segmentation Algorithms. *Ziraat Fakültesi Derg.* **2022**, *17*, 95–103. [CrossRef]

150. Beniaich, A.; Silva, M.L.N.; Guimarães, D.V.; Avalos, F.A.P.; Terra, F.S.; Menezes, M.D.; Avanzi, J.C.; Cândido, B.M. UAV-Based Vegetation Monitoring for Assessing the Impact of Soil Loss in Olive Orchards in Brazil. *Geoderma Reg.* **2022**, *30*, e00543. [CrossRef]

151. Salamí, E.; Gallardo, A.; Skorobogatov, G.; Barrado, C. On-the-Fly Olive Tree Counting Using a UAS and Cloud Services. *Remote Sens.* **2019**, *11*, 316. [CrossRef]

152. Jorge, J.; Vallbé, M.; Soler, J.A. Detection of Irrigation Inhomogeneities in an Olive Grove Using the NDRE Vegetation Index Obtained from UAV Images. *Eur. J. Remote Sens.* **2019**, *52*, 169–177. [CrossRef]

153. Safonova, A.; Guirado, E.; Maglinets, Y.; Alcaraz-Segura, D.; Tabik, S. Olive Tree Biovolume from UAV Multi-Resolution Image Segmentation with Mask R-CNN. *Sensors* **2021**, *21*, 1617. [CrossRef]

154. Alshammari, H.H.; Shahin, O.R. An Efficient Deep Learning Mechanism for the Recognition of Olive Trees in Jouf Region. *Comput. Intell. Neurosci.* **2022**, *2022*, e9249530. [CrossRef]

155. Papić, V.; Bugarin, N.; Gugić, J. On Olive Groves Analysis Using UAVs. In Proceedings of the 2021 International Conference on Software, Telecommunications and Computer Networks (SoftCOM), Hvar, Croatia, 23–25 September 2021; pp. 1–6.

156. Marques, P.; Pádua, L.; Sousa, J.; Fernandes-Silva, A. Assessment of UAV Thermal Imagery to Monitor Water Stress in Olive Trees. In Proceedings of the XXI International Horticultural Congress (IHC2022): International Symposium on Water: A Worldwide Challenge for Horticulture! Virtual Conference, 14 August 2022; pp. 157–164.

157. Ye, Z.; Wei, J.; Lin, Y.; Guo, Q.; Zhang, J.; Zhang, H.; Deng, H.; Yang, K. Extraction of Olive Crown Based on UAV Visible Images and the U2-Net Deep Learning Model. *Remote Sens.* **2022**, *14*, 1523. [CrossRef]

158. Yang, K.; Zhang, H.; Wang, F.; Lai, R. Extraction of Broad-Leaved Tree Crown Based on UAV Visible Images and OBIA-RF Model: A Case Study for Chinese Olive Trees. *Remote Sens.* **2022**, *14*, 2469. [CrossRef]

159. Marin, I.; Gotovac, S.; Papić, V. Individual Olive Tree Detection in RGB Images. In Proceedings of the 2022 International Conference on Software, Telecommunications and Computer Networks (SoftCOM), Split, Croatia, 22–24 September 2022; pp. 1–6.

160. Ottoy, S.; Tziolas, N.; Van Meerbeek, K.; Aravidis, I.; Tilkin, S.; Sismanis, M.; Stavrakoudis, D.; Gitas, I.Z.; Zalidis, G.; De Vocht, A. Effects of Flight and Smoothing Parameters on the Detection of Taxus and Olive Trees with UAV-Borne Imagery. *Drones* **2022**, *6*, 197. [CrossRef]

161. Catania, P.; Ferro, M.V.; Roma, E.; Orlando, S.; Vallone, M. Olive Tree Canopy Assessment Based on UAV Multispectral Images. In Proceedings of the AIIA 2022: Biosystems Engineering Towards the Green Deal; Ferro, V., Giordano, G., Orlando, S., Vallone, M., Cascone, G., Porto, S.M.C., Eds.; Springer International Publishing: Cham, Switzerland, 2023; pp. 469–478.

162. Catania, P.; Roma, E.; Orlando, S.; Vallone, M. Evaluation of Multispectral Data Acquired from UAV Platform in Olive Orchard. *Horticulturae* **2023**, *9*, 133. [CrossRef]

163. Roma, E.; Laudicina, V.A.; Vallone, M.; Catania, P. Application of Precision Agriculture for the Sustainable Management of Fertilization in Olive Groves. *Agronomy* **2023**, *13*, 324. [CrossRef]

164. Roma, E.; Catania, P.; Vallone, M.; Orlando, S. Unmanned Aerial Vehicle and Proximal Sensing of Vegetation Indices in Olive Tree (*Olea Europaea*). *J. Agric. Eng.* **2023**, 54. [CrossRef]

165. Dell'Anna, S.; Mansueto, G.; Boccardo, P.; Arco, E. Multi-Spectral Sensors Monitoring of the Epidemic of Xylella Fastidiosa in the Apulia Region. In Proceedings of the 2022 IEEE 21st Mediterranean Electrotechnical Conference (MELECON), Palermo, Italy, 14–16 June 2022; pp. 610–615.

166. Moreira, B.M.; Goyanes, G.; Pina, P.; Vassilev, O.; Heleno, S. Assessment of the Influence of Survey Design and Processing Choices on the Accuracy of Tree Diameter at Breast Height (DBH) Measurements Using UAV-Based Photogrammetry. *Drones* **2021**, *5*, 43. [CrossRef]

167. Fernández, T.; Gómez-Lopez, J.M.; Pérez-García, J.L.; Cardenal, J.; Delgado, J.; Mata, E.; Sánchez-Gómez, M.; Calero, J.; Tovar-Pescador, J.; Moya, F. Analysis of Gully Erosion in a Catchment Area in Olive Groves Using UAS Photogrammetry Techniques. *Int. Arch. Photogramm. Remote Sens. Spat. Inf. Sci.* **2020**, *XLIII-B2-2020*, 1057–1064. [CrossRef]

168. Santos-Rufo, A.; Mesas-Carrascosa, F.-J.; García-Ferrer, A.; Meroño-Larriva, J.E. Wavelength Selection Method Based on Partial Least Square from Hyperspectral Unmanned Aerial Vehicle Orthomosaic of Irrigated Olive Orchards. *Remote Sens.* **2020**, *12*, 3426. [CrossRef]

169. Šiljeg, A.; Panđa, L.; Domazetović, F.; Marić, I.; Gašparović, M.; Borisov, M.; Milošević, R. Comparative Assessment of Pixel and Object-Based Approaches for Mapping of Olive Tree Crowns Based on UAV Multispectral Imagery. *Remote Sens.* **2022**, *14*, 757. [CrossRef]

170. Castrignanò, A.; Belmonte, A.; Antelmi, I.; Quarto, R.; Quarto, F.; Shaddad, S.; Sion, V.; Muolo, M.R.; Ranieri, N.A.; Gadaleta, G.; et al. A Geostatistical Fusion Approach Using UAV Data for Probabilistic Estimation of *Xylella fastidiosa* Subsp. *Pauca* Infection in Olive Trees. *Sci. Total Environ.* **2021**, *752*, 141814. [CrossRef]

171. Belmonte, A.; Gadaleta, G.; Castrignanò, A. Use of Geostatistics for Multi-Scale Spatial Modeling of *Xylella fastidiosa* subsp. *pauca* (*Xfp*) Infection with Unmanned Aerial Vehicle Image. *Remote Sens.* **2023**, *15*, 656.

172. Ortega-Farías, S.; Ortega-Salazar, S.; Poblete, T.; Kilic, A.; Allen, R.; Poblete-Echeverría, C.; Ahumada-Orellana, L.; Zuñiga, M.; Sepúlveda, D. Estimation of Energy Balance Components over a Drip-Irrigated Olive Orchard Using Thermal and Multispectral Cameras Placed on a Helicopter-Based Unmanned Aerial Vehicle (UAV). *Remote Sens.* **2016**, *8*, 638. [CrossRef]

173. Lima-Cueto, F.J.; Blanco-Sepúlveda, R.; Gómez-Moreno, M.L.; Galacho-Jiménez, F.B. Using Vegetation Indices and a UAV Imaging Platform to Quantify the Density of Vegetation Ground Cover in Olive Groves (*Olea europaea* L.) in Southern Spain. *Remote Sens.* **2019**, *11*, 2564. [CrossRef]

174. Jurado, J.M.; Ortega, L.; Cubillas, J.J.; Feito, F.R. Multispectral Mapping on 3D Models and Multi-Temporal Monitoring for Individual Characterization of Olive Trees. *Remote Sens.* **2020**, *12*, 1106. [CrossRef]

175. Anifantis, A.S.; Camposeo, S.; Vivaldi, G.A.; Santoro, F.; Pascuzzi, S. Comparison of UAV Photogrammetry and 3D Modeling Techniques with Other Currently Used Methods for Estimation of the Tree Row Volume of a Super-High-Density Olive Orchard. *Agriculture* **2019**, *9*, 233. [CrossRef]

176. Sehree, N.A.; Khidhir, A.M. Olive Trees Cases Classification Based on Deep Convolutional Neural Network from Unmanned Aerial Vehicle Imagery. *Indones. J. Electr. Eng. Comput. Sci.* **2022**, *27*, 92–101.

177. Poblete-Echeverria, C.; Sepulveda-Reyes, D.; Ortega-Farias, S.; Zuniga, M.; Fuentes, S. Plant Water Stress Detection Based on Aerial and Terrestrial Infrared Thermography: A Study Case from Vineyard and Olive Orchard. In Proceedings of the XXIX International Horticultural Congress on Horticulture: Sustaining Lives, Livelihoods and Landscapes (IHC2014): 1112, Brisbane, Australia, 17 August 2014; pp. 141–146.

178. Avola, G.; Di Gennaro, S.F.; Cantini, C.; Riggi, E.; Muratore, F.; Tornambè, C.; Matese, A. Remotely Sensed Vegetation Indices to Discriminate Field-Grown Olive Cultivars. *Remote Sens.* **2019**, *11*, 1242. [CrossRef]

179. Zancanaro, E.; Gertsis, A.; Vellidis, G.; Marinello, F.; Morari, F. Developing Crop Canopy Model for Irrigation of High-Density Olive Groves by Using UAV Imagery. In *Precision Agriculture'19*; Wageningen Academic Publishers: Wageningen, The Netherlands, 2019; pp. 421–427. ISBN 978-90-8686-337-2.

180. Guillén-Climent, M.L.; Zarco-Tejada, P.J.; Villalobos, F.J. Estimating Radiation Interception in an Olive Orchard Using Physical Models and Multispectral Airborne Imagery. *Isr. J. Plant Sci.* **2012**, *60*, 107–121. [CrossRef]

181. Karydas, C.; Gewehr, S.; Iatrou, M.; Iatrou, G.; Mourelatos, S. Olive Plantation Mapping on a Sub-Tree Scale with Object-Based Image Analysis of Multispectral UAV Data; Operational Potential in Tree Stress Monitoring. *J. Imaging* **2017**, *3*, 57. [CrossRef]

182. Marques, P.; Pádua, L.; Brito, T.; Sousa, J.J.; Fernandes-Silva, A. Monitoring of Olive Trees Temperatures under Different Irrigation Strategies by UAV Thermal Infrared Imagery. In Proceedings of the IGARSS 2020—2020 IEEE International Geoscience and Remote Sensing Symposium, Waikoloa, HI, USA, 26 September–2 October 2020; pp. 4550–4553.

183. Iatrou, G.; Mourelatos, S.; Zartaloudis, Z.; Iatrou, M.; Gewehr, S.; Kalaitzopoulou, S. Remote Sensing for the Management of *Verticillium* Wilt of Olive. *Fresenius Environ. Bull.* **2016**, *25*, 3622–3628.

184. Šiljeg, A.; Marinović, R.; Domazetović, F.; Jurišić, M.; Marić, I.; Panđa, L.; Radočaj, D.; Milošević, R. GEOBIA and Vegetation Indices in Extracting Olive Tree Canopies Based on Very High-Resolution UAV Multispectral Imagery. *Appl. Sci.* **2023**, *13*, 739. [CrossRef]

185. Moorthy, I.; Miller, J.R.; Berni, J.A.J.; Zarco-Tejada, P.; Hu, B.; Chen, J. Field Characterization of Olive (*Olea europaea* L.) Tree Crown Architecture Using Terrestrial Laser Scanning Data. *Agric. For. Meteorol.* **2011**, *151*, 204–214. [CrossRef]

186. Melesse, A.M.; Weng, Q.; Thenkabail, P.S.; Senay, G.B. Remote Sensing Sensors and Applications in Environmental Resources Mapping and Modelling. *Sensors* **2007**, *7*, 3209–3241. [CrossRef] [PubMed]

187. Toth, C.; Jóźków, G. Remote Sensing Platforms and Sensors: A Survey. *ISPRS J. Photogramm. Remote Sens.* **2016**, *115*, 22–36. [CrossRef]

188. Austin, R. *Unmanned Aircraft Systems: UAVS Design, Development and Deployment*; John Wiley & Sons: Hoboken, NJ, USA, 2011; Volume 54, ISBN 1-119-96426-1.

189. Curran, P. Multispectral Remote Sensing of Vegetation Amount. *Prog. Phys. Geogr. Earth Environ.* **1980**, *4*, 315–341. [CrossRef]

190. Gerhards, M.; Schlerf, M.; Mallick, K.; Udelhoven, T. Challenges and Future Perspectives of Multi-/Hyperspectral Thermal Infrared Remote Sensing for Crop Water-Stress Detection: A Review. *Remote Sens.* **2019**, *11*, 1240. [CrossRef]

191. Khanal, S.; Fulton, J.; Shearer, S. An Overview of Current and Potential Applications of Thermal Remote Sensing in Precision Agriculture. *Comput. Electron. Agric.* **2017**, *139*, 22–32. [CrossRef]

192. Lee, W.S.; Alchanatis, V.; Yang, C.; Hirafuji, M.; Moshou, D.; Li, C. Sensing Technologies for Precision Specialty Crop Production. *Comput. Electron. Agric.* **2010**, *74*, 2–33. [CrossRef]

193. Koenig, K.; Höfle, B.; Hämmerle, M.; Jarmer, T.; Siegmann, B.; Lilienthal, H. Comparative Classification Analysis of Post-Harvest Growth Detection from Terrestrial LiDAR Point Clouds in Precision Agriculture. *ISPRS J. Photogramm. Remote Sens.* **2015**, *104*, 112–125. [CrossRef]

194. Padmavathi, K.; Thangadurai, K. Implementation of RGB and Grayscale Images in Plant Leaves Disease Detection—Comparative Study. *Indian J. Sci. Technol.* **2016**, *9*, 1–6. [CrossRef]

195. Zhao, T.; Stark, B.; Chen, Y.; Ray, A.L.; Doll, D. Challenges in Water Stress Quantification Using Small Unmanned Aerial System (sUAS): Lessons from a Growing Season of Almond. *J. Intell. Robot. Syst.* **2017**, *88*, 721–735. [CrossRef]

196. Calderón, R.; Navas-Cortés, J.A.; Lucena, C.; Zarco-Tejada, P.J. High-Resolution Airborne Hyperspectral and Thermal Imagery for Early Detection of *Verticillium* Wilt of Olive Using Fluorescence, Temperature and Narrow-Band Spectral Indices. *Remote Sens. Environ.* **2013**, *139*, 231–245. [CrossRef]

197. Deane, S.; Avdelidis, N.P.; Ibarra-Castanedo, C.; Zhang, H.; Nezhad, H.Y.; Williamson, A.A.; Mackley, T.; Maldague, X.; Tsourdos, A.; Nooralishahi, P. Comparison of Cooled and Uncooled IR Sensors by Means of Signal-to-Noise Ratio for NDT Diagnostics of Aerospace Grade Composites. *Sensors* **2020**, *20*, 3381. [CrossRef]

198. Omidi, R.; Moghimi, A.; Pourreza, A.; El-Hadedy, M.; Eddin, A.S. Ensemble Hyperspectral Band Selection for Detecting Nitrogen Status in Grape Leaves. In Proceedings of the 2020 19th IEEE International Conference on Machine Learning and Applications (ICMLA), Miami, FL, USA, 14–17 December 2020; pp. 286–293.

199. Morsy, S.; Shaker, A.; El-Rabbany, A. Multispectral LiDAR Data for Land Cover Classification of Urban Areas. *Sensors* **2017**, *17*, 958. [CrossRef]

200. Hugenholtz, C.H.; Whitehead, K.; Brown, O.W.; Barchyn, T.E.; Moorman, B.J.; LeClair, A.; Riddell, K.; Hamilton, T. Geomorphological Mapping with a Small Unmanned Aircraft System (sUAS): Feature Detection and Accuracy Assessment of a Photogrammetrically-Derived Digital Terrain Model. *Geomorphology* **2013**, *194*, 16–24. [CrossRef]

201. Whitehead, K.; Moorman, B.J.; Hugenholtz, C.H. Low-Cost, on-Demand Aerial Photogrammetry for Glaciological Measurement. *Cryosphere Discuss.* **2013**, *7*, 3043–3057.

202. Haala, N.; Cramer, M.; Weimer, F.; Trittler, M. Performance Test on Uav-Based Photogrammetric Data Collection. *ISPRS—Int. Arch. Photogramm. Remote Sens. Spat. Inf. Sci.* **2011**, *3822*, 7–12. [CrossRef]

203. Zhang, Y.; Xiong, J.; Hao, L. Photogrammetric Processing of Low-altitude Images Acquired by Unpiloted Aerial Vehicles. *Photogramm. Rec.* **2011**, *134*, 190–211. [CrossRef]

204. Crommelinck, S.; Bennett, R.; Gerke, M.; Nex, F.; Yang, M.Y.; Vosselman, G. Review of Automatic Feature Extraction from High-Resolution Optical Sensor Data for UAV-Based Cadastral Mapping. *Remote Sens.* **2016**, *8*, 689. [CrossRef]

205. Jay, S.; Rabatel, G.; Hadoux, X.; Moura, D.; Gorretta, N. In-Field Crop Row Phenotyping from 3D Modeling Performed Using Structure from Motion. *Comput. Electron. Agric.* **2015**, *110*, 70–77. [CrossRef]

206. Arefi, H.; d'Angelo, P.; Mayer, H.; Reinartz, P. *Automatic Generation of Digital Terrain Models from Cartosat-1 Stereo Images*; Heipke, C., Jacobsen, K., Müller, S., Sörgel, U., Eds.; ISPRS: Hannover, Germany, 2009; Volume 83, pp. 1–6.

207. Turner, D.; Lucieer, A.; Wallace, L. Direct Georeferencing of Ultrahigh-Resolution UAV Imagery. *IEEE Trans. Geosci. Remote Sens.* **2014**, *52*, 2738–2745. [CrossRef]

208. Hamuda, E.; Glavin, M.; Jones, E. A Survey of Image Processing Techniques for Plant Extraction and Segmentation in the Field. *Comput. Electron. Agric.* **2016**, *125*, 184–199. [CrossRef]

209. Shinde, P.P.; Shah, S. *A Review of Machine Learning and Deep Learning Applications*; IEEE: Piscataway, NJ, USA, 2018; pp. 1–6.

210. Marques, P.; Pádua, L.; Adão, T.; Hruška, J.; Peres, E.; Sousa, A.; Sousa, J.J. UAV-Based Automatic Detection and Monitoring of Chestnut Trees. *Remote Sens.* **2019**, *11*, 855. [CrossRef]

211. Rasmussen, J.; Ntakos, G.; Nielsen, J.; Svensgaard, J.; Poulsen, R.N.; Christensen, S. Are Vegetation Indices Derived from Consumer-Grade Cameras Mounted on UAVs Sufficiently Reliable for Assessing Experimental Plots? *Eur. J. Agron.* **2016**, *74*, 75–92. [CrossRef]

212. Woebbecke, D.M.; Meyer, G.E.; Von Bargen, K.; Mortensen, D. Color Indices for Weed Identification under Various Soil, Residue, and Lighting Conditions. *Trans. ASAE* **1995**, *38*, 259–269. [CrossRef]

213. Gitelson, A.A.; Kaufman, Y.J.; Stark, R.; Rundquist, D. Novel Algorithms for Remote Estimation of Vegetation Fraction. *Remote Sens. Environ.* **2002**, *80*, 76–87. [CrossRef]

214. Salamí, E.; Barrado, C.; Pastor, E. UAV Flight Experiments Applied to the Remote Sensing of Vegetated Areas. *Remote Sens.* **2014**, *6*, 11051–11081. [CrossRef]

215. Dunford, R.; Michel, K.; Gagnage, M.; Piégay, H. Potential and Constraints of Unmanned Aerial Vehicle Technology for the Characterization of Mediterranean Riparian Forest. *Int. J. Remote Sens.* **2009**, *30*, 4915–4935. [CrossRef]

216. Hung, C.; Bryson, M.; Sukkarieh, S. Multi-Class Predictive Template for Tree Crown Detection. *ISPRS J. Photogramm. Remote Sens.* **2012**, *68*, 170–183. [CrossRef]

217. Sugiura, R.; Noguchi, N.; Ishii, K. Remote-Sensing Technology for Vegetation Monitoring Using an Unmanned Helicopter. *Biosyst. Eng.* **2005**, *90*, 369–379. [CrossRef]

218. Baluja, J.; Diago, M.P.; Balda, P.; Zorer, R.; Meggio, F.; Morales, F.; Tardaguila, J. Assessment of Vineyard Water Status Variability by Thermal and Multispectral Imagery Using an Unmanned Aerial Vehicle (UAV). *Irrig. Sci.* **2012**, *30*, 511–522. [CrossRef]

219. Zarco-Tejada, P.J.; González-Dugo, V.; Berni, J.A.J. Fluorescence, Temperature and Narrow-Band Indices Acquired from a UAV Platform for Water Stress Detection Using a Micro-Hyperspectral Imager and a Thermal Camera. *Remote Sens. Environ.* **2012**, *117*, 322–337. [CrossRef]

220. Zecha, C.W.; Link, J.; Claupein, W. Mobile Sensor Platforms: Categorisation and Research Applications in Precision Farming. *J. Sens. Sens. Syst.* **2013**, *2*, 51–72. [CrossRef]

221. Turner, D.; Lucieer, A.; Watson, C. An Automated Technique for Generating Georectified Mosaics from Ultra-High Resolution Unmanned Aerial Vehicle (UAV) Imagery, Based on Structure from Motion (SfM) Point Clouds. *Remote Sens.* **2012**, *4*, 1392–1410. [CrossRef]

222. Martínez-Ruedas, C.; Yanes Luis, S.; Díaz-Cabrera, J.M.; Gutiérrez Reina, D.; Galvín, A.P.; Castillejo-González, I.L. Convolutional Neural Networks for Planting System Detection of Olive Groves. In *Innovations in Machine and Deep Learning: Case Studies and Applications*; Rivera, G., Rosete, A., Dorronsoro, B., Rangel-Valdez, N., Eds.; Studies in Big Data; Springer Nature: Cham, Switzerland, 2023; pp. 373–399. ISBN 978-3-031-40688-1.

223. Hossain, M.D.; Chen, D. Segmentation for Object-Based Image Analysis (OBIA): A Review of Algorithms and Challenges from Remote Sensing Perspective. *ISPRS J. Photogramm. Remote Sens.* **2019**, *150*, 115–134. [CrossRef]

224. Chen, X.; Ishwaran, H. Random Forests for Genomic Data Analysis. *Genomics* **2012**, *99*, 323–329. [CrossRef]

225. Mountrakis, G.; Im, J.; Ogole, C. Support Vector Machines in Remote Sensing: A Review. *ISPRS J. Photogramm. Remote Sens.* **2011**, *66*, 247–259. [CrossRef]

226. Waleed, M.; Um, T.-W.; Khan, A.; Ahmad, Z. An Automated Method for Detection and Enumeration of Olive Trees through Remote Sensing. *IEEE Access* **2020**, *8*, 108592–108601. [CrossRef]

227. Khan, A.; Khan, U.; Waleed, M.; Khan, A.; Kamal, T.; Marwat, S.N.K.; Maqsood, M.; Aadil, F. Remote Sensing: An Automated Methodology for Olive Tree Detection and Counting in Satellite Images. *IEEE Access* **2018**, *6*, 77816–77828. [CrossRef]

228. Kotsiantis, S.B. Decision Trees: A Recent Overview. *Artif. Intell. Rev.* **2013**, *39*, 261–283. [CrossRef]

229. Waleed, M.; Um, T.-W.; Khan, A.; Khan, U. Automatic Detection System of Olive Trees Using Improved K-Means Algorithm. *Remote Sens.* **2020**, *12*, 760. [CrossRef]

230. Sutton, C.; McCallum, A. An Introduction to Conditional Random Fields. *Found. Trends® Mach. Learn.* **2012**, *4*, 267–373. [CrossRef]

231. Abozeid, A.; Alanazi, R.; Elhadad, A.; Taloba, A.I.; Abd El-Aziz, R.M. A Large-Scale Dataset and Deep Learning Model for Detecting and Counting Olive Trees in Satellite Imagery. *Comput. Intell. Neurosci.* **2022**, *2022*, e1549842. [CrossRef] [PubMed]

232. Martínez-Ruedas, C.; Yanes-Luis, S.; Díaz-Cabrera, J.M.; Gutiérrez-Reina, D.; Linares-Burgos, R.; Castillejo-González, I.L. Detection of Planting Systems in Olive Groves Based on Open-Source, High-Resolution Images and Convolutional Neural Networks. *Agronomy* **2022**, *12*, 2700. [CrossRef]

233. Chemin, Y.H.; Beck, P.S.A. A Method to Count Olive Trees in Heterogenous Plantations from Aerial Photographs. *Preprints* **2017**, 2017100170. [CrossRef]

234. Peña-Barragán, J.M.; Jurado-Expósito, M.; López-Granados, F.; Atenciano, S.; Sánchez-de la Orden, M.; García-Ferrer, A.; García-Torres, L. Assessing Land-Use in Olive Groves from Aerial Photographs. *Agric. Ecosyst. Environ.* **2004**, *103*, 117–122. [CrossRef]

235. Sepulcre-Cantó, G.; Zarco-Tejada, P.J.; Sobrino, J.A.; Berni, J.A.J.; Jiménez-Muñoz, J.C.; Gastellu-Etchegorry, J.P. Discriminating Irrigated and Rainfed Olive Orchards with Thermal ASTER Imagery and DART 3D Simulation. *Agric. For. Meteorol.* **2009**, *149*, 962–975. [CrossRef]

236. Gitelson, A.A.; Kaufman, Y.J.; Merzlyak, M.N. Use of a Green Channel in Remote Sensing of Global Vegetation from EOS-MODIS. *Remote Sens. Environ.* **1996**, *58*, 289–298. [CrossRef]

237. Idso, S.B.; Jackson, R.D.; Pinter, P.J.; Reginato, R.J.; Hatfield, J.L. Normalizing the Stress-Degree-Day Parameter for Environmental Variability. *Agric. Meteorol.* **1981**, *24*, 45–55. [CrossRef]

238. Daughtry, C.S.T.; Walthall, C.L.; Kim, M.S.; de Colstoun, E.B.; McMurtrey, J.E. Estimating Corn Leaf Chlorophyll Concentration from Leaf and Canopy Reflectance. *Remote Sens. Environ.* **2000**, *74*, 229–239. [CrossRef]

239. Broge, N.H.; Leblanc, E. Comparing Prediction Power and Stability of Broadband and Hyperspectral Vegetation Indices for Estimation of Green Leaf Area Index and Canopy Chlorophyll Density. *Remote Sens. Environ.* **2001**, *76*, 156–172. [CrossRef]

240. Ben-Gal, A.; Agam, N.; Alchanatis, V.; Cohen, Y.; Yermiyahu, U.; Zipori, I.; Presnov, E.; Sprintsin, M.; Dag, A. Evaluating Water Stress in Irrigated Olives: Correlation of Soil Water Status, Tree Water Status, and Thermal Imagery. *Irrig. Sci.* **2009**, *27*, 367–376. [CrossRef]

241. Zarco-Tejada, P.J.; Diaz-Varela, R.; Angileri, V.; Loudjani, P. Tree Height Quantification Using Very High Resolution Imagery Acquired from an Unmanned Aerial Vehicle (UAV) and Automatic 3D Photo-Reconstruction Methods. *Eur. J. Agron.* **2014**, *55*, 89–99. [CrossRef]

242. Díaz-Varela, R.; de la Rosa, R.; León, L.; Zarco-Tejada, P. High-Resolution Airborne UAV Imagery to Assess Olive Tree Crown Parameters Using 3D Photo Reconstruction: Application in Breeding Trials. *Remote Sens.* **2015**, *7*, 4213–4232. [CrossRef]

243. Zarco-Tejada, P.J.; Miller, J.R.; Morales, A.; Berjón, A.; Agüera, J. Hyperspectral Indices and Model Simulation for Chlorophyll Estimation in Open-Canopy Tree Crops. *Remote Sens. Environ.* **2004**, *90*, 463–476. [CrossRef]

244. Estornell, J.; Ruiz, L.A.; Velázquez-Martí, B.; López-Cortés, I.; Salazar, D.; Fernández-Sarría, A. Estimation of Pruning Biomass of Olive Trees Using Airborne Discrete-Return LiDAR Data. *Biomass Bioenergy* **2015**, *81*, 315–321. [CrossRef]

245. Hadaś, E.; Estornell, J. Accuracy of Tree Geometric Parameters Depending on the LiDAR Data Density. *Eur. J. Remote Sens.* **2016**, *49*, 73–92. [CrossRef]

246. Reyes-González, A.; Kjaersgaard, J.; Trooien, T.; Hay, C.; Ahiablame, L. Comparative Analysis of METRIC Model and Atmometer Methods for Estimating Actual Evapotranspiration. *Int. J. Agron.* **2017**, *2017*, e3632501. [CrossRef]

247. Ramírez-Cuesta, J.M.; Allen, R.G.; Zarco-Tejada, P.J.; Kilic, A.; Santos, C.; Lorite, I.J. Impact of the Spatial Resolution on the Energy Balance Components on an Open-Canopy Olive Orchard. *Int. J. Appl. Earth Obs. Geoinf.* **2019**, *74*, 88–102. [CrossRef]

248. Cammalleri, C.; Anderson, M.C.; Ciraolo, G.; D'Urso, G.; Kustas, W.P.; La Loggia, G.; Minacapilli, M. Applications of a Remote Sensing-Based Two-Source Energy Balance Algorithm for Mapping Surface Fluxes without in Situ Air Temperature Observations. *Remote Sens. Environ.* **2012**, *124*, 502–515. [CrossRef]

249. Cammalleri, C.; Ciraolo, G.; Minacapilli, M.; Rallo, G. Evapotranspiration from an Olive Orchard Using Remote Sensing-Based Dual Crop Coefficient Approach. *Water Resour. Manag.* **2013**, *27*, 4877–4895. [CrossRef]

250. Cawse-Nicholson, K.; Braverman, A.; Kang, E.L.; Li, M.; Johnson, M.; Halverson, G.; Anderson, M.; Hain, C.; Gunson, M.; Hook, S. Sensitivity and Uncertainty Quantification for the ECOSTRESS Evapotranspiration Algorithm—DisALEXI. *Int. J. Appl. Earth Obs. Geoinf.* **2020**, *89*, 102088. [CrossRef]

251. Norman, J.M.; Kustas, W.P.; Humes, K.S. Source Approach for Estimating Soil and Vegetation Energy Fluxes in Observations of Directional Radiometric Surface Temperature. *Agric. For. Meteorol.* **1995**, *77*, 263–293. [CrossRef]

252. Minacapilli, M.; Agnese, C.; Blanda, F.; Cammalleri, C.; Ciraolo, G.; D'Urso, G.; Iovino, M.; Pumo, D.; Provenzano, G.; Rallo, G. Estimation of Actual Evapotranspiration of Mediterranean Perennial Crops by Means of Remote-Sensing Based Surface Energy Balance Models. *Hydrol. Earth Syst. Sci.* **2009**, *13*, 1061–1074. [CrossRef]

253. Riveros-Burgos, C.; Ortega-Farías, S.; Morales-Salinas, L.; Fuentes-Peñailillo, F.; Tian, F. Assessment of the Clumped Model to Estimate Olive Orchard Evapotranspiration Using Meteorological Data and UAV-Based Thermal Infrared Imagery. *Irrig. Sci.* **2021**, *39*, 63–80. [CrossRef]

254. Kaufman, Y.J.; Tanre, D. Atmospherically Resistant Vegetation Index (ARVI) for EOS-MODIS. *IEEE Trans. Geosci. Remote Sens.* **1992**, *30*, 261–270. [CrossRef]

255. Rondeaux, G.; Steven, M.; Baret, F. Optimization of Soil-Adjusted Vegetation Indices. *Remote Sens. Environ.* **1996**, *55*, 95–107. [CrossRef]

256. Di Nisio, A.; Adamo, F.; Acciani, G.; Attivissimo, F. Fast Detection of Olive Trees Affected by Xylella Fastidiosa from UAVs Using Multispectral Imaging. *Sensors* **2020**, *20*, 4915. [CrossRef]

257. Gamon, J.A.; Peñuelas, J.; Field, C.B. A Narrow-Waveband Spectral Index That Tracks Diurnal Changes in Photosynthetic Efficiency. *Remote Sens. Environ.* **1992**, *41*, 35–44. [CrossRef]

258. Zarco-Tejada, P.J.; Berjón, A.; López-Lozano, R.; Miller, J.R.; Martín, P.; Cachorro, V.; González, M.R.; de Frutos, A. Assessing Vineyard Condition with Hyperspectral Indices: Leaf and Canopy Reflectance Simulation in a Row-Structured Discontinuous Canopy. *Remote Sens. Environ.* **2005**, *99*, 271–287. [CrossRef]

259. Ksibi, A.; Ayadi, M.; Soufiene, B.O.; Jamjoom, M.M.; Ullah, Z. MobiRes-Net: A Hybrid Deep Learning Model for Detecting and Classifying Olive Leaf Diseases. *Appl. Sci.* **2022**, *12*, 10278. [CrossRef]

260. Wang, Q.; Nuske, S.; Bergerman, M.; Singh, S. Automated Crop Yield Estimation for Apple Orchards. In *Experimental Robotics: The 13th International Symposium on Experimental Robotics*; Desai, J.P., Dudek, G., Khatib, O., Kumar, V., Eds.; Springer Tracts in Advanced Robotics; Springer International Publishing: Berline/Heidelberg, Germany, 2013; pp. 745–758, ISBN 978-3-319-00065-7.

261. Azpiroz, I.; Oses, N.; Quartulli, M.; Olaizola, I.G.; Guidotti, D.; Marchi, S. Comparison of Climate Reanalysis and Remote-Sensing Data for Predicting Olive Phenology through Machine-Learning Methods. *Remote Sens.* **2021**, *13*, 1224. [CrossRef]

262. Sghaier, A.; Dhaou, H.; Jarray, L.; Abaab, Z.; Sekrafi, A.; Ouessar, M. Assessment of Drought Stress in Arid Olive Groves Using HidroMORE Model. *J. Agric. Eng.* **2022**, *53*. [CrossRef]

263. Weissteiner, C.J.; Strobl, P.; Sommer, S. Assessment of Status and Trends of Olive Farming Intensity in EU-Mediterranean Countries Using Remote Sensing Time Series and Land Cover Data. *Ecol. Indic.* **2011**, *11*, 601–610. [CrossRef]

264. Hadas, E.; Borkowski, A.; Estornell, J.; Tymkow, P. Automatic Estimation of Olive Tree Dendrometric Parameters Based on Airborne Laser Scanning Data Using Alpha-Shape and Principal Component Analysis. *GIScience Remote Sens.* **2017**, *54*, 898–917. [CrossRef]

265. Agam, N.; Cohen, Y.; Berni, J.A.J.; Alchanatis, V.; Kool, D.; Dag, A.; Yermiyahu, U.; Ben-Gal, A. An Insight to the Performance of Crop Water Stress Index for Olive Trees. *Agric. Water Manag.* **2013**, *118*, 79–86. [CrossRef]